Effects of Ultrasonic Transducers on Heat Transfer in Packed Particle Beds

A Thesis Presented for the
Master of Science
Degree
The University of Tennessee, Knoxville

David Patrick Moseley
December 2016

ACKNOWLEDGEMENTS

I would like to thank my committee chair, Dr. Matthew Mench, who has been incredibly generous with his knowledge and time. His humor, advice and continually positive attitude are inspiring.

I would also like to thank Dr. Ayyoub Momen for creating a research environment that was both challenging and rewarding. Without his guidance and persistent support this thesis would not have been possible.

Additionally, I would like to thank my committee members, Dr. David Irick and Dr. Kivanc Ekici, whose support throughout graduate school has been steadfast and invaluable.

ABSTRACT

The objective of this study was to determine the effects of ultrasonic transducers on heat transfer in a packed particle bed heat exchanger. Although substantial research has been devoted to ultrasound, and the associated improvements in heat transfer, data regarding the effects on packed particle beds is non-existent. This is of particular interest given the potential to improve heat transfer in a wide variety of packed particle bed systems. A 42.9% increase in the heat transfer rate was demonstrated as the result of improved fluid convection throughout the packed particle bed. Secondary effects, including acoustic cavitation, acoustic streaming and local agitation, may have also contributed to the improved heat transfer rate.

TABLE OF CONTENTS

Introduction 1
Chapter 1: Background 4
Packed Particle Beds 4
Ultrasonic Transducers 5
Ultrasonic-Transducer-Enhanced-Heat-Transfer 8
Phase Change 9
Boiling 9
Food Industry/Drying 10
Convection 11
Chapter 2: Gravity-Fed System (1st setup) 13
Tube-to-Particle-Diameter 13
Materials and Methods 14
Results and Discussion 16
Chapter 3: Copper Tube Packed Bed (2nd setup) 21
Materials and Methods 21
Results and Discussion 22
Chapter 4: Updated Copper PPB Design (3rd setup) 24
Materials and Methods 24
Data Collection 27
Experimental Procedure 27
Results and Discussion 27
Chapter 5: PPB Design with Dampener (4th setup) 39
Methods and Materials 39
Data Collection 40
Experimental Procedure 40
Results and Discussion 42
Isolation Valve 44
Chapter 6: Final Design (5th setup) 48
Materials and Methods 48
Data Collection 50
Particle Selection 50
Pressure Drop 53
Time Constant 55
Experimental Procedure 57
Results and Discussion 60
Conclusions 74
List of References 75
Vita 78

LIST OF TABLES

Table 1 Test Data w/o UTs Energized…… 18
Table 2 Test Data with UTs Energized……... 19
Table 3 Pump Flow Rates…….26
Table 4 Stainless Steel Particle Distribution…….. 51
Table 5 Particle Density Data……...53
Table 6 Pressure Data……...62
Table 7 Pressure Data Error…….62
Table 8 Time Constant Comparison……... 69

LIST OF FIGURES

Figure 1 Packed Particle Bed Reactor Schematic 2
Figure 2 PZT Crystal Structure 6
Figure 3 Piezoelectric Effects 7
Figure 4 Gravity-fed System Design 16
Figure 5 Temperature Profile w/o UTs Energized 17
Figure 6 Temperature Profile with UTs Energized 18
Figure 7 Temperature Data with Pulsed Ultrasonic Transducers 20
Figure 8 Copper PPB Heat Transfer Comparison 23
Figure 9 Updated PPB System Design (3rd setup) 26
Figure 10 200 ml/min: Temperature Data UTs On 28
Figure 11 200 ml/min:Temperature Data UTs Off 28
Figure 12 200 ml/min: DTC dT/dt 29
Figure 13 400 ml/min: Temperature Data UTs On 30
Figure 14 400 ml/min: Temperature Data UTs Off 31
Figure 15 400 ml/min: DTC dT/dt 31
Figure 16 650 ml/min: Temperature Data UTs On 32
Figure 17 650 ml/min: Temperature Data UTs Off 32
Figure 18 650 ml/min: DTC dT/dt 33
Figure 19 1200 ml/min: Temperature Data UTs On 33
Figure 20 1200 ml/min: Temperature Data UTs Off 34
Figure 21 1200 ml/min: dT/dt 34
Figure 22 Pressure Data Flow Rate 1 36
Figure 23 Pressure Data Flow Rate 2 36
Figure 24 Pressure Data Flow Rate 3 37
Figure 25 Pressure Data Flow Rate 4 37
Figure 26 PPB Design with Dampener 41
Figure 27 Pressure Fluctuations without Dampener 43
Figure 28 Pressure Fluctuations with Dampener 43
Figure 29 Warm-up Temperature Curves with Dampener 45
Figure 30 Pressure Data with Isolation Valve 45
Figure 31 Temperature Data with Isolation Valve 46
Figure 32 Particle Size Distribution 52
Figure 33 Final PPB Design 58
Figure 34 Flow Diagram: Warm-up cycle 58
Figure 35 Flow Diagram: Initial cool-down cycle 59
Figure 36 Flow Diagram: Cool-down testing 59
Figure 37 Pressure Drop with UTs OFF 60
Figure 38 Pressure Drop with UTs ON 61
Figure 39 Pressure Drop Comparison Using Ergun Equation 62
Figure 40 Modified Reynolds Number Data 63
Figure 41 Friction Factor versus Tube-to-Particle Diameter 64

Figure 42 **200 ml/min:** Temperature Data with UTs Energized 65
Figure 43 **200 ml/min:** Temperature Data without UTs Energized 65
Figure 44 **200 ml/min:** DTC Comparison 66
Figure 45 **400 ml/min:** Temperature Data with UTs Energized 66
Figure 46 **400 ml/min:** Temperature Data without UTs Energized 67
Figure 47 **400 ml/min:** DTC Comparison 67
Figure 48 **600 ml/min:** Temperature Data with UTs Energized 68
Figure 49 **600 ml/min:** Temperature Data without UTs Energized 68
Figure 50 **600 ml/min:** DTC Comparison 69
Figure 51 Temperature Time Constant Comparison 72
Figure 52 Temperature Time Constant Comparison: Ultrasonic Transducers Off 72
Figure 53 Temperature Time Constant Comparison: Ultrasonic Transducers ON 73

INTRODUCTION

Packed Particle Beds

Packed particle beds are found in a wide variety of industrial and commercial applications and play an important role in water purification, pharmaceutical manufacturing, the chemical industry and others. As one of the most common reactors available, research focused on improving packed particle bed (PPB) reactors has great potential and widespread applicability. Packed particle beds typically consist of hollow vessels filled with various packing materials ranging from catalyst particles to absorbents, and are arranged in either a structured or random fashion. The intent of a PPB is to provide enhanced contact in multi-phase systems. In chemical reactors, fluid flows through the packed catalyst particles and ultimately results in changes to the chemical composition of the system. Applications of PPBs typically include absorption, distillation, catalytic reactions, fluidized beds, magnetocaloric refrigeration, and others. As one of the most efficient chemical reactor systems available its use is widespread. Figure 1 provides insight to a typical PPB reactor design.

Ultrasonic Transducers

Ultrasonic transducers are formed using piezoelectric materials, which are typically ceramics composed of metal oxides. These materials are permanently polarized and exhibit electrostrictive properties allowing them to either produce a voltage under mechanical force or vice versa. When an inverting voltage source,

usually in the form of a direct current square wave, is applied across the UT, the material expands and contracts. Consequently, ultrasonic transducers are well suited to displace bulk fluids and are used in this study to improve convection within the PPB.

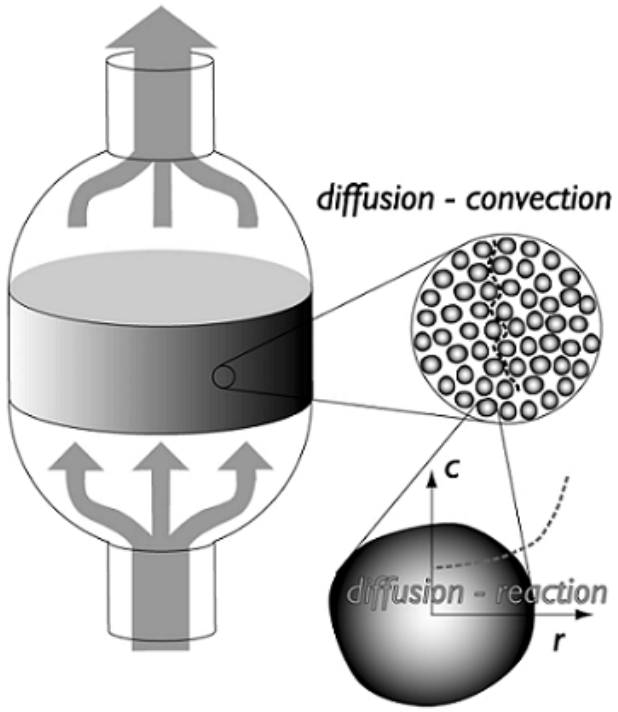


Figure 1 Packed Particle Bed Reactor Schematic

In general, the dissipation of acoustic energy imparts momentum which ultimately results in fluid motion. This forced convection is utilized to improve the heat transfer coefficient within the PPB system primarily via acoustic streaming with secondary effects such as acoustic cavitation and local agitation also contributing to changes in the heat transfer characteristics.

Ultrasonic-Transducer-Enhanced Heat Transfer

Work related to the effects of ultrasonic vibrations can be found as early as the 60s which serve as the essential pioneer studies. Unfortunately, these studies provided mixed, inconclusive results. Until the 90s, data regarding ultrasonic vibrations and heat transfer was virtually non-existent, however, interest has steadily increased with the number of related publications increasing four fold in the past decade. Research topics have involved the effects of ultrasonic vibrations on melting, solidification, boiling, drying and fluid convection. By far, the effects of ultrasonic vibrations on fluid convection, and the resultant improvements in heat transfer, are the most common. Improvements in prior studies range from 20% to over 8 times the heat transfer rate depending on the system configuration and applied power.

CHAPTER 1: BACKGROUND

Packed Particle Beds

Although particle beds are common due to their high conversion rate, they suffer from several fluid and heat transfer related issues. Near-wall fluid bypass, which is a function of a more structured particle distribution, results in greater void fraction and alters heat transfer, mass transport and flow characteristics(Achenbach 1995). Where uniform spheres come in contact with the wall, fluid channels are created which results in an uneven velocity distribution and an overall decrease in fluid contact with packing particles. Hotspots are also common due to convective instability and non-homogenous fluid flow(Yakhnin and Menzinger 1998).

Literature also confirms that although “randomly” packed beds are, in general, random, it is important to considered the fact that hydraulic and mechanical shocks can cause permanent alterations to the particle distribution depending on how the bed was treated prior to testing. Specifically, clusters have been shown to form in the interior of the bed which further alters the mass transport and heat transfer characteristics(Barker 1965).

There are numerous design challenges that must be overcome in order to ensure cost effective implementation of packed particle bed systems. Understanding mass transport, heat transfer as well as the various chemical reactions is essential to proper design. In the process of understanding various designs, modelling can be useful. However, choosing how to model the catalyst

particle is important to the overall model accuracy and must be carefully considered.

Additionally, designing to minimize pressure drop is important as it effects intraparticle diffusion, chemical reaction time as well as the size of pumps used in forced convection systems. Larger particle sizes result in minimal pressure drop. Conversely, smaller particles reduce void fraction, permeability and many other attributes which can negatively affect performance. The typical particle size is around 1mm although there are numerous designs utilizing other sizes. As a basic point of reference, the space between packing particles is defined as the macroporous structure and the pores of the particles themselves as the microstructure.

Ultrasonic Transducers

At the core of piezoelectric materials, the same materials used to produce ultrasonic transducers, is the concept of spontaneous polarization. This is a result of the shifting of atoms from a baseline position and gives the linear, piezoelectric materials their unique properties. These dipole moments are a function of the natural angular momentum of the material's constituent particles which are aligned in a given direction producing a permanent magnetization. The most common ferroelectric materials used in piezoelectric transducers are from the perovskite structure. Lead zirconate titanate, also known as PZT, is a ceramic perovskite material that exhibits piezoelectric properties and is frequently used for ultrasonic transducers. As can be seen in Figure 2, the displacement of

the Ti^{+4} ion is responsible for the asymmetric structure and thus the permanent polarization. As will be discussed later in terms of design considerations, an appropriate Curie temperature must be selected in order to insure a strong polarization during operation. As the transducer's temperature increases, the excitation energy of the polarizing electrons increases which alters, spin and location ultimately destroying the polarization (Safari, 2008). This depolarization increases as the operating temperature approaches the Curie temperature at which point the material assumes a centrosymmetric, paraelectric state and is no longer polarized.

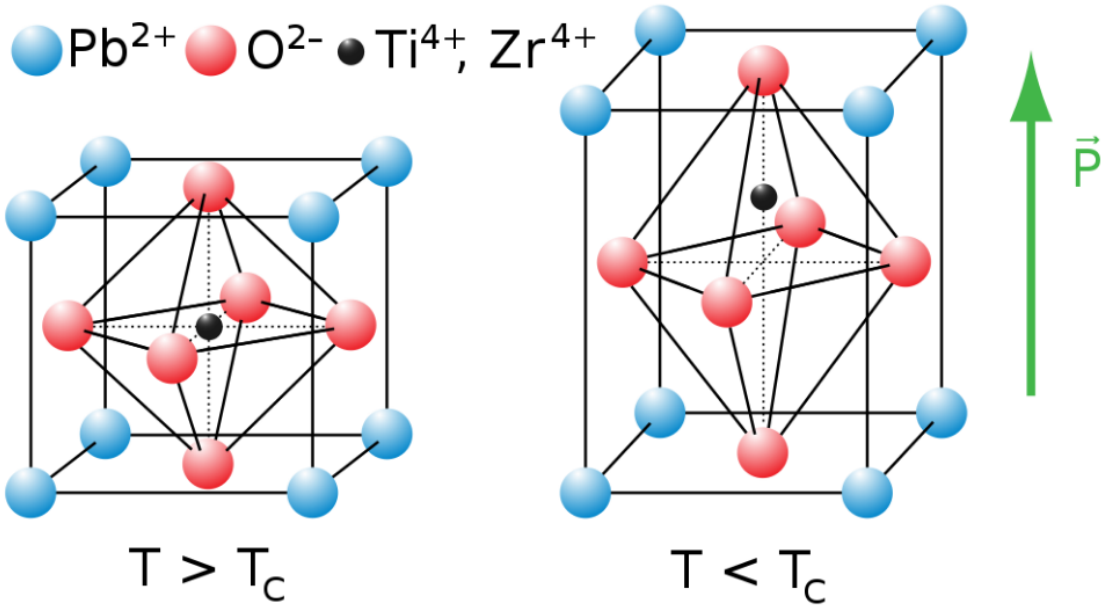


Figure 2 PZT Crystal Structure

Another fundamental concept associated the polarization of ferroelectrics is spontaneous strain. In general, the polarization vector and strain tensor align

which causes an electrostrictive coupling in the material (Safari, 2008). This electrostrictive property is responsible for the expansion and contraction of the piezoelectric transducers. This can be thought of as the conversion of electrical energy to mechanical energy.

Given that this is a reversible process, the ultrasonic transducers can both produce electricity when mechanically stressed and vice versa as can be seen in Figure 3. This has led to a wide variety of applications utilizing piezoelectric materials. The reversibility of ferroelectrics, also known as ferroelectric hysteresis, occurs when the material is subjected to an electric field. Under the electric field the direction of the polarization vector switches as the electric field is applied.

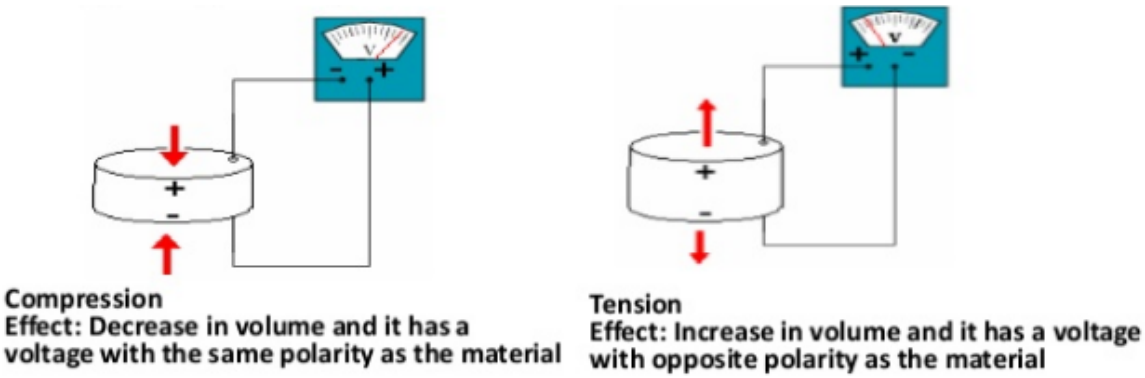


Figure 3 Piezoelectric Effects

Because the polarization vectors are generally oriented in a parallel fashion, the vector switching can easily occur. This material property allows ferroelectrics to become piezoelectric through a process called poling. This

process involves subjecting the material to a strong magnetic field which forces the polarization vectors to align near the electric field. As the electric field increases, the polarization will increase until the material reaches a saturation state. Once the magnetic field is removed, the vectors remain generally aligned in the direction of the previously-applied electric field and is called the remnant polarization; however, the alignment is not perfectly unidirectional.

Ultrasonic-Transducer-Enhanced-Heat-Transfer

Although the research in this thesis was performed using cylindrical ceramic discs as the piezoelectric transducer, numerous other designs are available and have been used to improve heat transfer. For example, the heat transfer characteristics of a cylindrical surface exposed to a piezoelectric fan was explored and substantial improvements shown. The piezoelectric material was attached to a thin flexible blade used to improve heat transfer in low convective regions. The results showed a 1.2 to 2.4 times improvement in the heat transfer coefficient. Additionally, the augmented local heat transfer coefficient was increase 2.85 times (Chien-Nan Lin.) Alternatively, an increasing amount of research has been focused on the effects of piezoelectric transducers on heat transfer in heat exchangers. Ye Yao et. al. attached a single transducer to the outside of a water-water shell-and-tube heat exchanger operating at a frequency of 21kHz at power settings of 40 watts, 60 watts and 100 watts. The study found that improvements decreased with an increase in water flow rate and increased with an increase in power. The improvements were minimal compared to other

research and were between 8% and 17%. However, it's important to note that the type of transducer used, frequency of operation and power all greatly affect results. In the case of Ye Yao et al, a UT normally used for cleaning was used and the frequency and power were much lower than other studies.

Phase Change

In one study, the effects of ultrasound on the freezing rate of potatoes was considered. A 13% improvement in freezing rate was observed with the frequency set at 25kHz at a power of 15.85 W. The study showed the exposure time to ultrasound as an important parameter considering the thermal effects created by passing ultrasonic waves through the medium. In another study, the use of ultrasound to promote a phase change from super cooled water to ice was found to have a significant impact and allowed the researchers to tune when the phase transition occurred (Takaaki Inada, Xu Zhang.)

Boiling

In other studies, it has been shown that UTs can significantly improve heat transfer. In particular, up to an eight-fold increase in the heat transfer coefficient was achieved in natural convection (S.W. Wong, W.Y. Wong.) Several studies site cavitation as the primary mechanism responsible for the improvements. Specifically, during initial stages of boiling the nucleation sites are excited away from the surface which reduces film boiling and improves the overall heat transfer.

In another study, Jeong et al found an 87-126% increase in the critical heat flux when ultrasonic vibrations were applied to the heated plate surface. The angle of inclination significantly affected the changes in critical heat flux with the maximum effects appearing with a downward facing orientation. The authors hypothesized that ultrasonic waves impacting the plate surface disrupted the vapor film assisting in the escape of the vapor away from the surface. Similarly, good agreement with (Jeong) is found in a study involving subcooled boiling conditions. Up to a 67% increase in heat transfer was observed utilizing ultrasound at frequencies ranging from 37kHz to 40kHz and 300-500 W (Carlo Bartoli.)

Food Industry/Drying

Efforts to increase the lifespan of various food products has led to the use of ultrasound to improve the drying process without permanently altering, or in some cases damaging, the food item. The most common method of drying uses heat, however, many food products suffer from adverse effects under increased temperature. In order to avoid the use of heat in the drying process, ultrasound can be used. Specifically, two primary mechanisms exist to enhance the heat transfer process—vibration via direct contact and external modifications to the acoustic field. In direct contact methods the ultrasonic transducers cause the expansion and contraction of the material which leads to improved heat transfer. Design considerations that use the direct contact method include the porosity of

the material as well as impedance matching. In the case of externally applied acoustic fields, improvements effect the moisture diffusivity and are greatest at low air velocities (de la Fuente-Blanco, 2006 Gallego-Juarez,1999.)

Convection

Although research regarding the effects of ultrasonic transducers on convective heat transfer represent the majority of literature, no experiments have been conducted with UTs integrated into packed particle beds. However, improvements have been shown in systems where various liquids are subjected to sound waves in the ultrasonic power band. For example, researchers documented a 20% increase in the heat flux of saturated ethyl alcohol in the presence of ultrasonic waves at a frequency of 28kHz and 33.6 watts (Iida). It was concluded the improvements were a result of improved convection. In other research, improvements to the heat transfer coefficient in a liquid bath were shown to be almost 2 times higher with the use of ultrasonic transducers operated at frequencies between 20kHz and 60kHz (Kim.) It was also shown that the flow regime significantly altered the heat transfer improvements.

For systems involving heat exchangers, ultrasonic transducers not only improve the heat transfer rate, but also reduce fouling. All experiments to date involve ultrasonic transducers integrated externally to the system in contrast to the internal integration found in this study. For example, one experiment studied the heat transfer effects of a copper coil passing cold fluid through a stationary hot bath. The system utilized transducers operating at a frequency range of

20kHz to 1.6Mhz. The heat transfer coefficient increased up to two fold (Monnot.) Gondrexon, et.al explored the effects of vibrating a shell-and-tube heat exchanger at a resonant frequency of 35kHz which resulted in a 260% increase in the heat transfer coefficient. It is important to note that researchers found that, of the 100 watts applied to the transducer, 70%-75% was absorbed by the liquid.

CHAPTER 2: GRAVITY-FED SYSTEM (1ST SETUP)

In order to expedite the process of testing the effects of ultrasonic transducers on heat transfer, a basic design was chosen. Given that this research was partly influenced by an industry partner, geometric restrictions were provided, and limited the shaped and diameter of the test system.

In industry, packed particle beds range in sizes from half a meter to over several meters in diameter. Similarly, the length of PPBs varies widely, and will depend on the reaction requirements and several other factors. In the first phase of this study, the system was designed as a baseline representation of a more complex heat transfer system currently under research and subject to confidentiality agreements. The results of this research can provide valuable direction for further study.

Tube-to-Particle-Diameter

The PPB design utilized a 76.4 mm long tube with an inner diameter of 13.7 mm and outer diameter of 16 mm. Given the size of the inside diameter, the selection of particle size was critical. In general, PPBs with low tube-to-particle-diameter ratios, $\frac{\mathrm{D}}{\mathrm{dp}}$, suffer from several negative performance issues. Specifically, the more structured arrangement of particles near the tube wall causes increases in porosity, permeability and ultimately non-homogenous fluid flow.

Under the above circumstances, assumptions which neglect the near-wall viscous effects are no longer valid as both the friction caused by the particles and the tube wall must be accounted for. Generally, particle viscous friction dominates for tube-to-particle-diameter ratios greater than 4 (Winterberg and Tsotsas 2000). The iron particles used in the first test system ranged from .25 mm to .66 mm which provided a $\frac{D}{dp}$ range of approximately 20 to 55.

In each of the following chapters, the various design iterations and improvements will be explored including discussion of the results and any modifications required.

Materials and Methods

In order to reduce the time required to develop a PPB prototype and produce useable data, a simple gravity-feed design was chosen. Flexible tubing was selected to house the thermocouple, ultrasonic transducers as well as the iron particles. The flexible tubing was selected as an inexpensive and readily available option which allowed for simple integration of the UTs and offered a straightforward sealing process.

Three Stem Inc. ultrasonic transducers with a resonance frequency of 135 kHz were integrated at equal distance along the tube. The transducers were powered by a T&C Power Conversions Inc. AG Series Amplifier which was capable of recovering reflected power and provided measurements of forward, reflected and load power. The amplifier provided control variables including forward power as well as frequency. Although the amplifier is suitable for use

with a signal generator, all tests were performed using the built-in sinusoidal waveform. The waveform, amplitude and frequency were verified using a Tektronix DPO 4034 digital phosphor oscilloscope.

The electrode surfaces were sealed using epoxy as they were exposed to the flowing liquid. A precision fine-wire Omega t-type copper-constantan thermocouple of diameter .08 mm was used at the outlet. The outlet thermocouple was mounted at the exit such that it maintained a position at the center of fluid flow.

A Synthware reflux condenser was used as a heat exchanger to produce the cold bath used for the heat transfer testing. The condenser was connected in series with a Lauda Brinkmann EcoLine Re106 chiller which provided a glycol coolant to maintain a 10°C cold water bath within the condenser. The output was connected via Norprene tubing to a brass shut-off valve which was then connected directly to the flexible PPB. Liquid was collected in a 500 ml graduated cylinder.

Once the cold bath reached the 10°C temperature, tests were performed with and without the UTs energized. Briefly, the PPB was allowed to reach a uniform temperature matching ambient air. The cut-off valve was then actuated to allow the cold bath fluid to flow through the PPB while data was collected.

Temperature data was recorded via LabView using a data acquisition system. Figure 4 provides a basic schematic of the experimental setup.

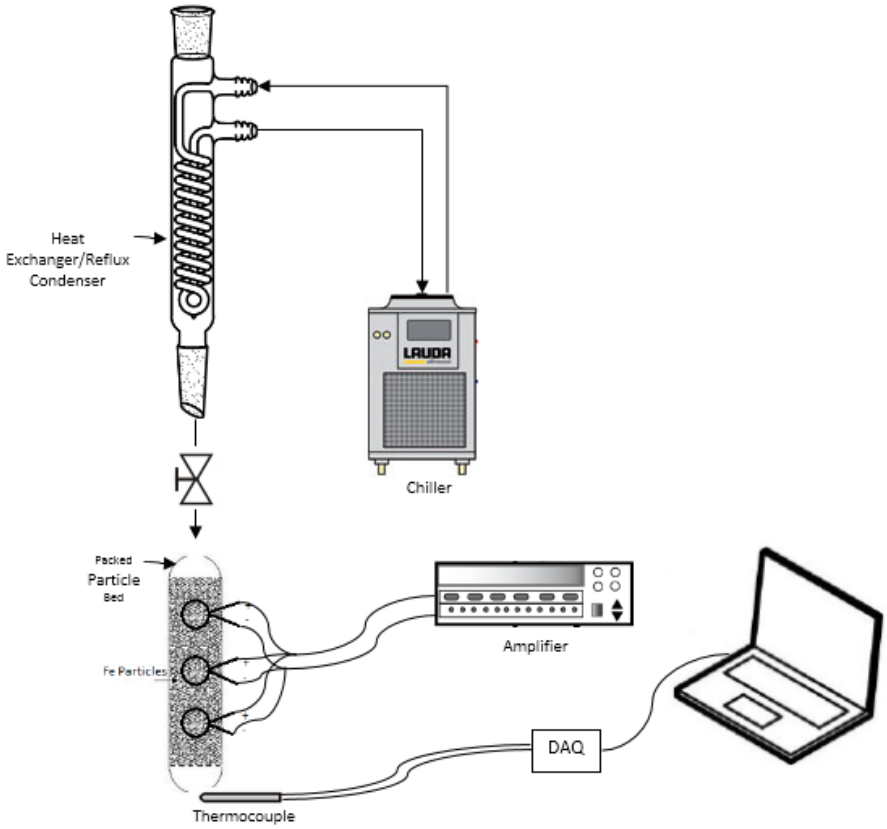


Figure 4 Gravity-fed System Design

Results and Discussion

The initial tests produced the expected heat transfer curve and were conducted with the ultrasonic transducers turned off. The final temperature never reached the targeted 10°C temperature due to heat loss along the length of tubing, due to the thermal mass of the brass valve as well as an insufficient cold bath liquid volume of 349 ml. Figure 5 provides a graphical representation of the data collected for temperature changes without the ultrasonic transducers energized.

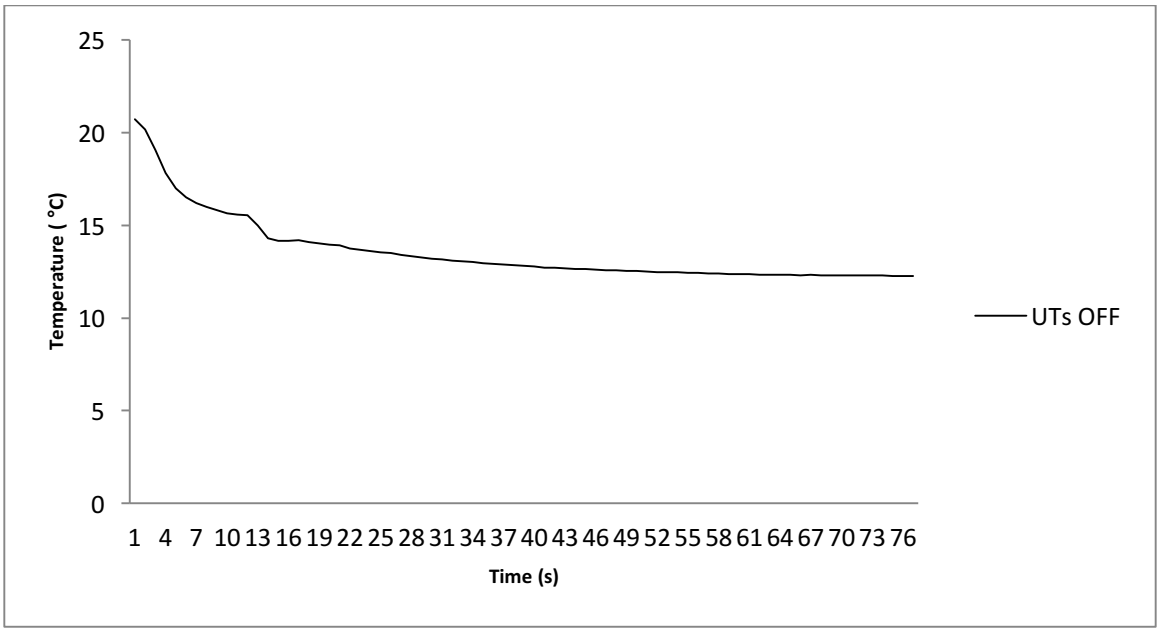


Figure 5 Temperature Profile w/o UTs Energized

Subsequent testing was conducted in the same manner, however, the ultrasonic transducers were energized.

Figure 6 provides graphical insight to the test results and Table 1 highlights important data from the initial tests. As can be seen from

Figure 6, the temperature profile behaved as expected, however the thermocouple readings indicated an approximate 20°C temperature increase compared to the tests without the UTs energized. It was determined that the ultrasonic transducers were not properly sealed which resulted in the applied voltage leaking into the water. This excess voltage was transmitted through the thermocouple and resulted in the inaccurate temperature readings. It is important to notice the drop in temperature at the end of the test once the transducers were turned off.

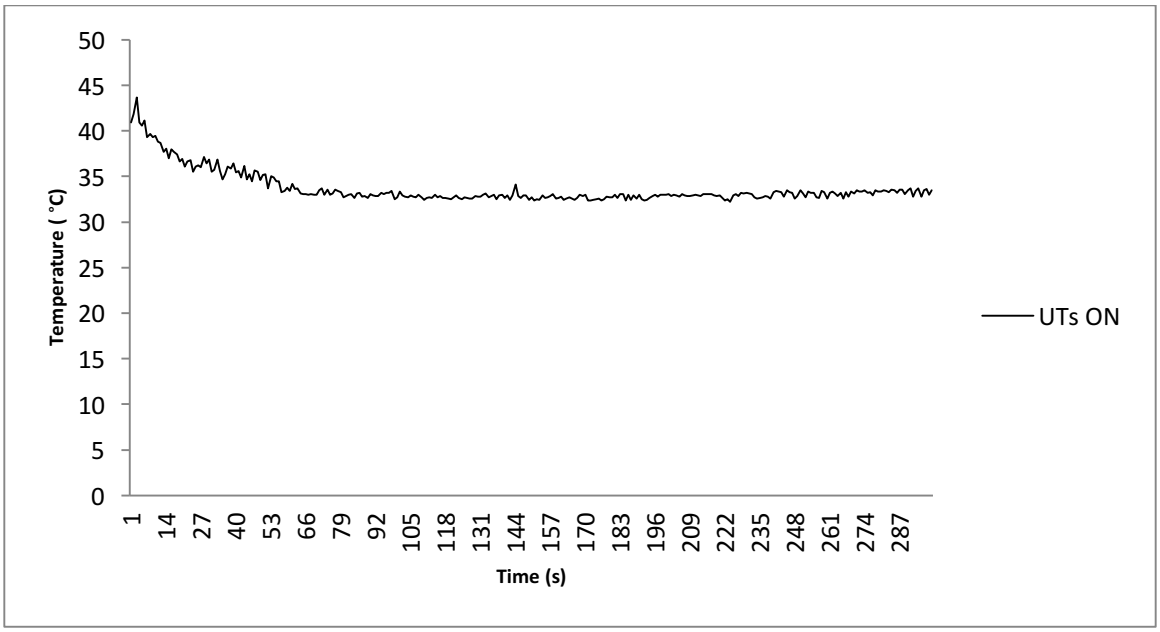


Figure 6 Temperature Profile with UTs Energized

Table 1 Test Data w/o UTs Energized

Total test time :	258.732 seconds
Volume filtered and collected:	348.5 ml
Average Flow Rate:	1.346 ml/s
Lowest Temperature Reached	12.05°C

As can be seen in Table 2, the flow rate was significantly less than initial tests. The change in flow rate could have been a result of using the UTs, however, subsequent tests proved this to be untrue. Instead, it's more likely that the iron particles shifted which resulted in a change in the porosity.

In order to verify the assumption that voltage from the transducers was altering the temperature reading, additional tests were performed. During the tests, temperature was monitored without the use of the UTs during the cool-down of the PPB. Following the cool-down portion, the UTs were pulsed on and off. Figure 7 shows the thermocouple data collected during the above-mentioned tests. It can be seen that during the periods when the UTs were energized the data shows a spike in temperature.

Table 2 Test Data with UTs Energized

Time to filter water:	567.228 seconds
Volume filtered and collected:	348 ml
Average Flow Rate:	.6135 ml/s
Lowest Temperature Reached	32.20°C
Frequency	135 kHz
Power Setting	2 watts
Forward Power (FP)	2 watts
Reflected Power (RP)	1 watt
Load Power (LP)	1 watt

In addition to the challenges experienced due to the inaccurate temperature readings, the pressure head created by the cold bath did not produce a substantial flow rate through the PPB; nor could the flow rate be accurately controlled. Consequently, the system design required modifications to allow for the use of a high pressure water source as well as the ability to accurately capture temperature data. 0 provides information on the subsequent modifications and results.

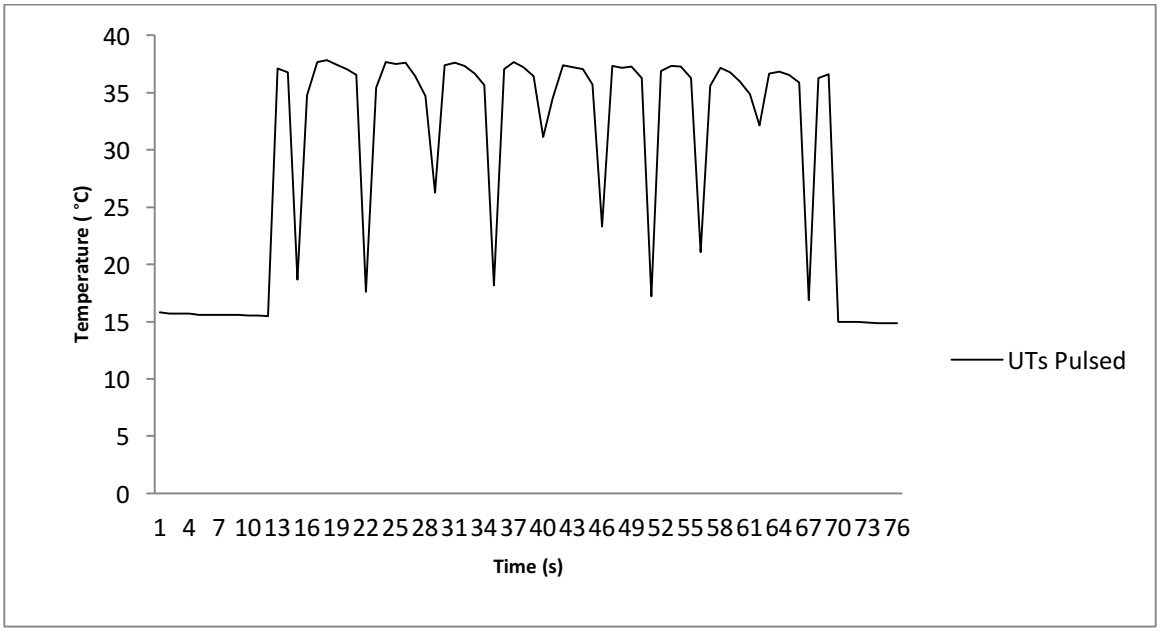


Figure 7 Temperature Data with Pulsed Ultrasonic Transducers

CHAPTER 3: COPPER TUBE PACKED BED (2ND SETUP)

The gravity-feed system suffered from several drawbacks and required modifications. The second prototype utilized copper tubing which provided improved structural rigidity and access to 70 pisg water pressure. In the gravity-fed testing, measurements were made as the PPB transitioned from room temperature to 10°C, however, the copper PPB system was designed with the opposite in mind. The entire PPB was first chilled and then data was collected as it transitioned to room temperature.

Materials and Methods

The same components were integrated into the copper PPB as with the gravity-fed system and included UTs, a thermocouple as well as iron particles. The ends of the system were sealed using stainless steel mesh and the entire system was then connected to a sink faucet which provided sufficient pressures for varied flow rates. The different flow rates were measured experimentally and the corresponding valve settings were documented. At this point in the experimentation process, data showing the transient temperature profiles with the UTs energized had not been collected. This was due to design flaws with the initial prototype.

Results and Discussion

The primary objective was to determine if the UTs provided improved heat transfer, and if so, additional efforts would focus on a more advanced and refined test system.

Although the design utilized 3 ultrasonic transducers with a maximum power rating of 2.2 watts each, the UTs were only powered by 2 watts total. In comparison to data found in literature, this power rating was substantially lower. Previous research shows the use of surface-mounted UTs exclusively and power ranges from 50-350 watts.

Given the minimal amount of power supplied to the UTs, it was expected the improvements would be less than those found previous works. As can be seen in Figure 8, the temperature data shows a noticeably faster rate with the UTs energized. Although the data captured during these tests did not include upstream temperature readings or pressure data, the results satisfied the acceptance criteria and confirmed additional, more refined testing should be performed. 0 discusses the design improvements and associated test results.

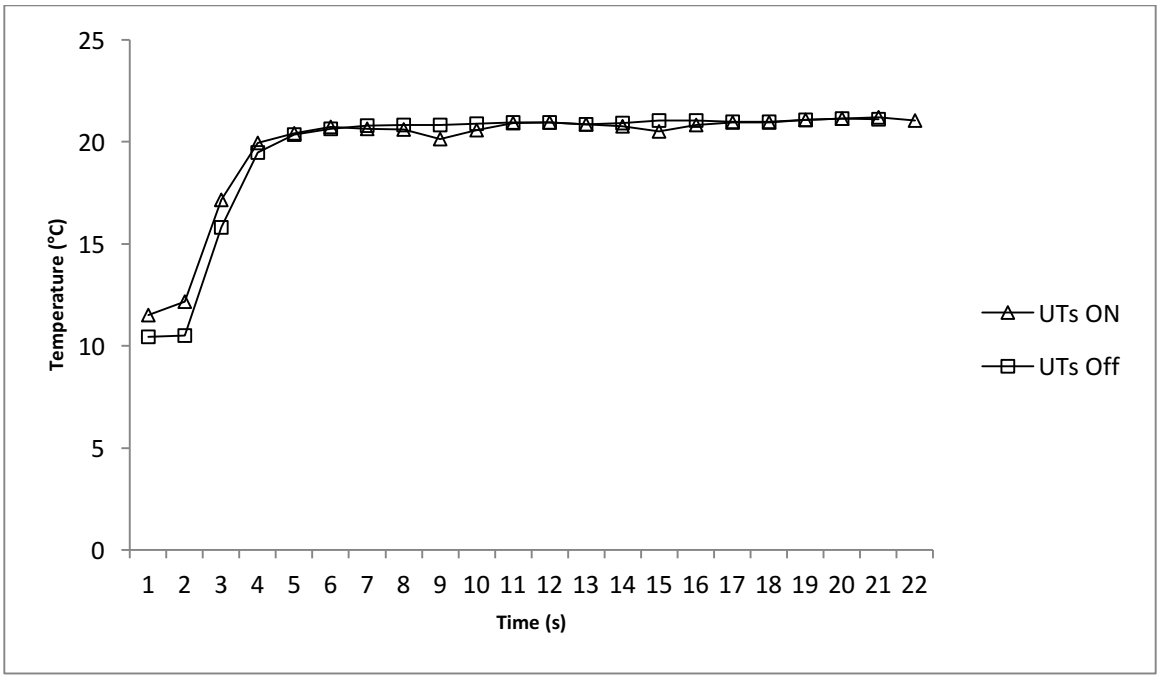


Figure 8 Copper PPB Heat Transfer Comparison

CHAPTER 4: UPDATED COPPER PPB DESIGN (3RD SETUP)

With the initial tests results showing a notable difference in the heat transfer rate, design improvements were made and additional tests were performed. Similar to the first prototype design, the second system design lacked testing flexibility and was not capable of collecting all the necessary data required to verify improvements in heat transfer. Consequently, several design changes were made to improve the quality and flexibility of the system.

Materials and Methods

The previous design required substantial amounts of time between each test. During this time, the PPB was allowed to reach thermal equilibrium with the chiller water at 10 °C. Additionally, the previous system did not allow for data to be collected during both a cool-down cycle and warm-up cycle. In order to reduce the time between each data set as well as provided data on both the cooling and warming of the system, the process was changed. Instead of cooling the entire PPB, the Synthware reflux condenser, used in previous test, was integrated in-line with the chiller as a heat exchanger to provide a cold bath. As before, this cold water was then passed through the PPB and temperature data was collected.

In order to further reduce test cycle time, and provide heat transfer data during a warm-up cycle, a warm bath was used. This design change was accomplished using two, stainless steel shut-off valves integrated upstream of a

peristaltic pump. Each valve was connected to either the warm or cold bath and only one valve was open at a time. This allowed for both the warm and cold baths to be simultaneously connected to the pump.

Given the repeatability difficulties producing an exact flow rate using the faucet valve settings, a Cole-Palmer Masterflex Easy-Load peristaltic pump, model 7518-10 was integrated into the system. The pump used ¼" inside diameter tubing with a range of 6-600 rpm. This provided a reliable and consistent flow rate which was essential to improving the test data quality.

As previous tests did not include pressure readings, a Omegadyne pressure transducer with a pressure range of 0-200 psi and an output voltage of 0-5V was used. Prior to testing, the pressure transducer was calibrated and scaled accordingly in LabView.

In order to more accurately and completely characterize the heat transfer within the PPB, an additional Omega t-type thermocouple, identical to the downstream thermocouple, was integrated at the inlet of the PPB. Figure 9 outlines the updated system design.

The testing procedure was initiated by setting the pump at one of the four different flow rates. The flow rate data is provided in Table 3 and ranged from 200 ml/min to 1200 ml/min. Testing at higher flow rates was performed in order to determine the point at which the UTs no longer provided heat transfer enhancement. Subsequent tests used this data to tune the flow rates to the range which resulted in heat transfer improvements.

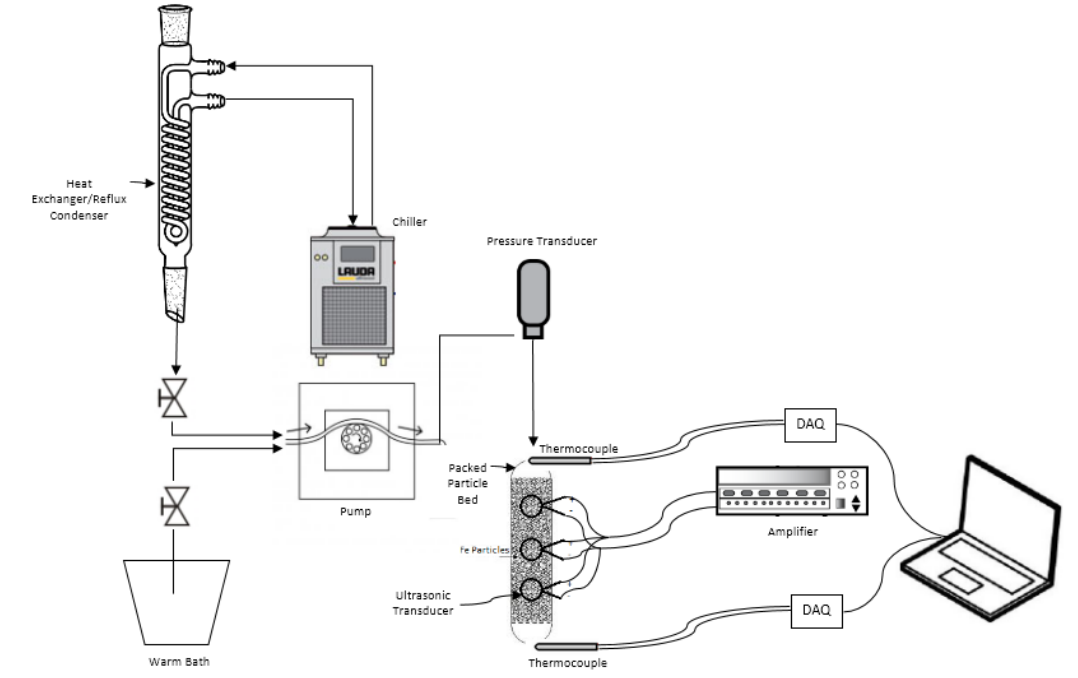


Figure 9 Updated PPB System Design (3rd setup)

Table 3 Pump Flow Rates

Flow	**Rate ($\frac{ml}{min}$)**
1	200
2	400
3	650
4	1200

Data Collection

Data from the pressure transducer was collected via a National Instruments NI9201 module with a voltage accuracy of .015 volts and sampling rate of 500 kS/s. Analog thermocouple readings were collected utilizing a National Instruments 9213 module with 50Hz/60Hz noise rejection and up to .02 °C temperature sensitivity. All data was process using LabVIEW with a sampling rate of 10 Hz.

Experimental Procedure

Initially, the cold bath valve was closed and warm water was passed through the PPB to bring the system to thermal equilibrium. Once the upstream and downstream thermocouples reached equilibrium, the warm-bath valve was closed and the cold-bath valve was opened. The cold water was passed through the system until the cold-bath volume was exhausted. Once the cold bath was emptied, the valve was closed and the warm-bath valve was then opened. The system was allowed to return to room temperature.

Results and Discussion

Data from all 4 flow rates is provided below. As can be seen in Figure 10, the data shows the expected curves associated with the cooling and heating cycles. It is difficult to visualize the difference in the temperature curves found in Figure 11 due to disturbances in the upstream thermocouple. Subsequent tests at other flow rates did not suffer from this variance.

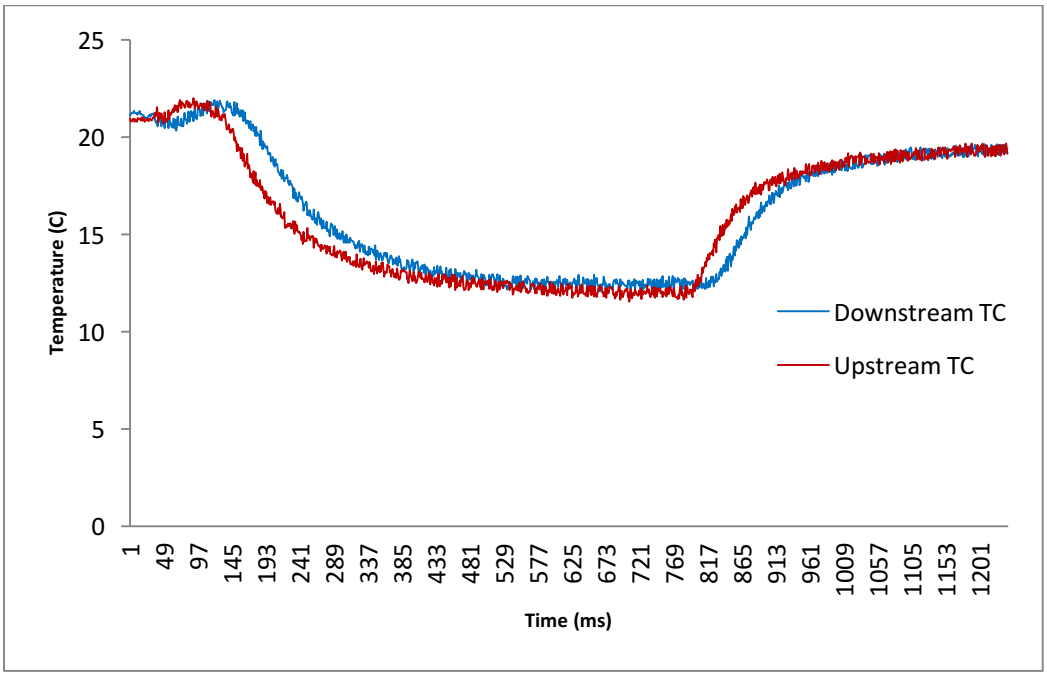


Figure 10 200 ml/min: Temperature Data UTs On

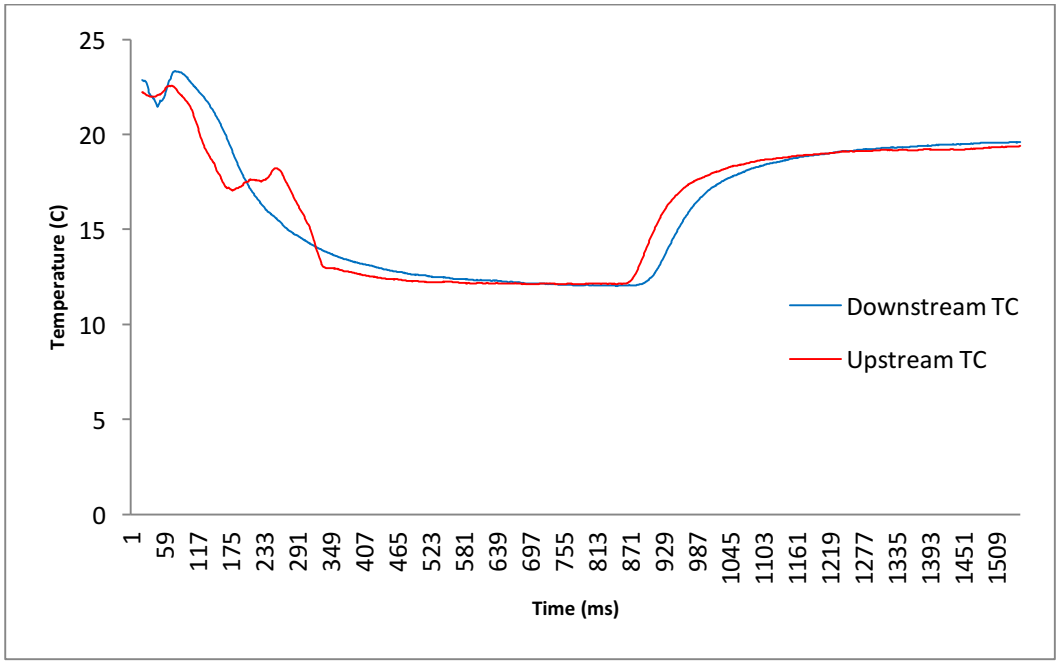


Figure 11 200 ml/min:Temperature Data UTs Off

It is not immediately obvious from visual inspection if the heat transfer is improved with the use of UTs, however, taking the derivative of the downstream thermocouple data from both data sets and plotting them together provides more insight. It is apparent from Figure 12 that the downstream temperature change occurred faster when the UTs were energized. The improvement in heat transfer also occurs at the second flow rate tested. The results from higher flow rates, however, show that the UTs exhibit a decreasing impact on heat transfer as expected. The ultrasonic transducers are set at a fixed power, and as the flow rate increases, the ability of the transducers to improve turbulence within the PPB decreases.

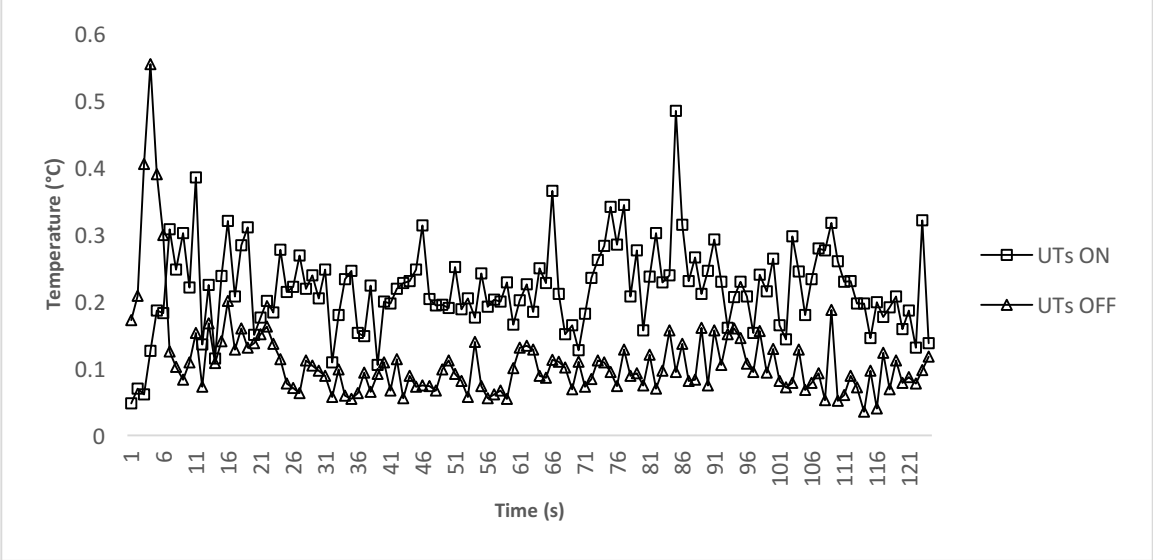


Figure 12 200 ml/min: DTC dT/dt

In order to experience similar improvements in heat transfer at higher flow rates, the UTs must receive more power. It is also possible to add additional UTs

to the system. This would allow the UTs to remain in the lower limits of their power ratings which would minimize heat generation while simultaneously increasing the ability to displace fluid within the PPB. Future experiments will utilize higher power inputs as well as an increased number of UTs.

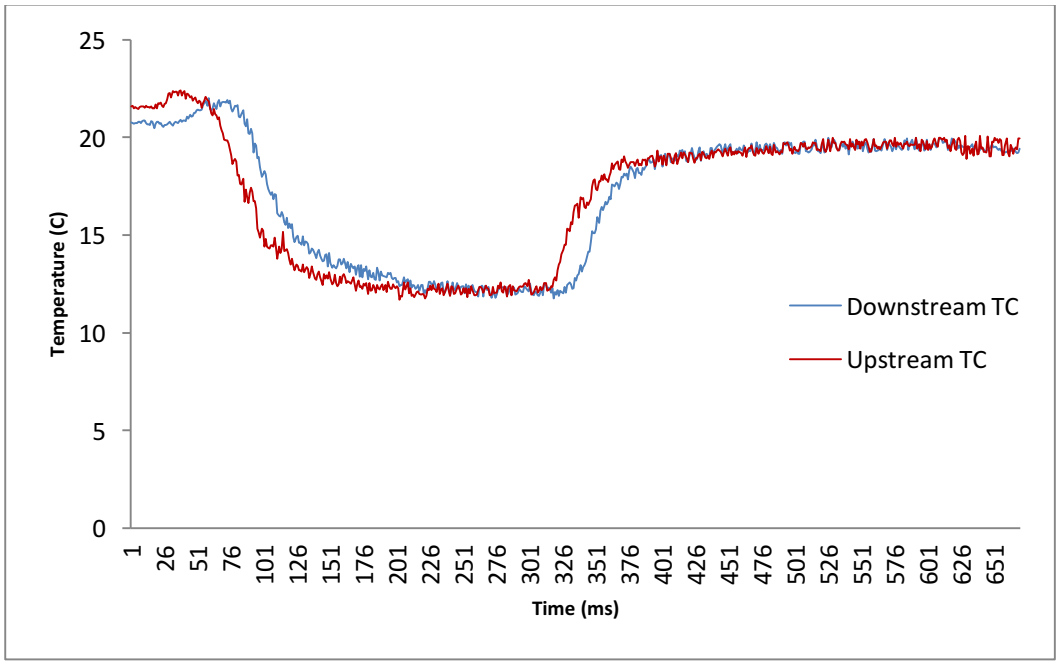


Figure 13 400 ml/min: Temperature Data UTs On

It is important to note the sporadic fluctuations in the thermocouple data. For flow rates above 200 ml/min, the data exhibits undesirable noise. After analyzing the pressure transducer data, it was determined that the fluctuations were directly related to the pump used.

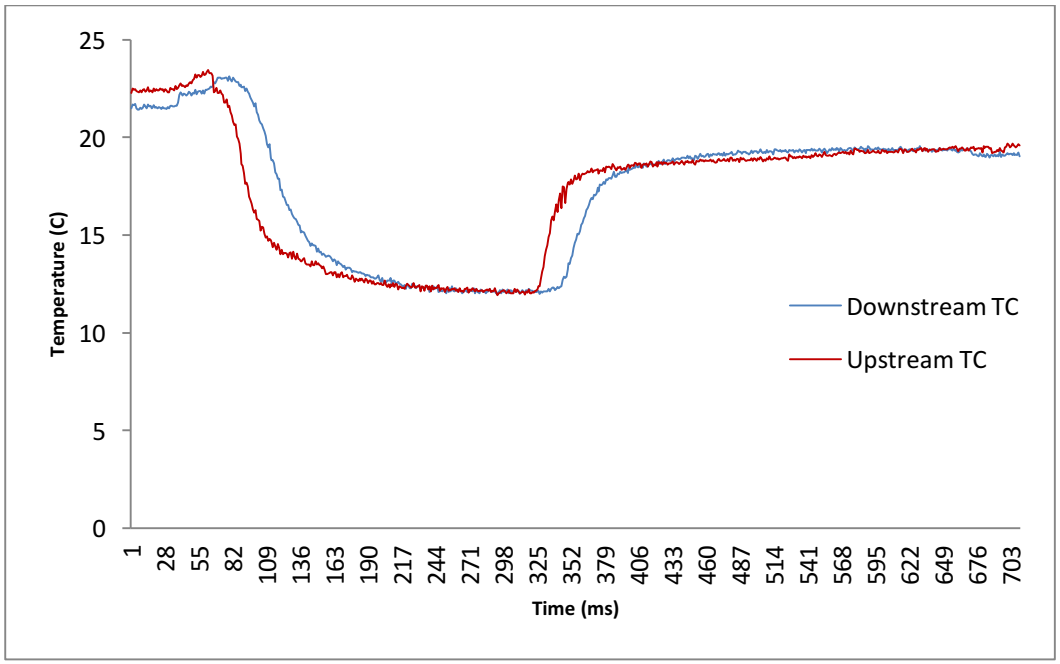


Figure 14 400 ml/min: Temperature Data UTs Off

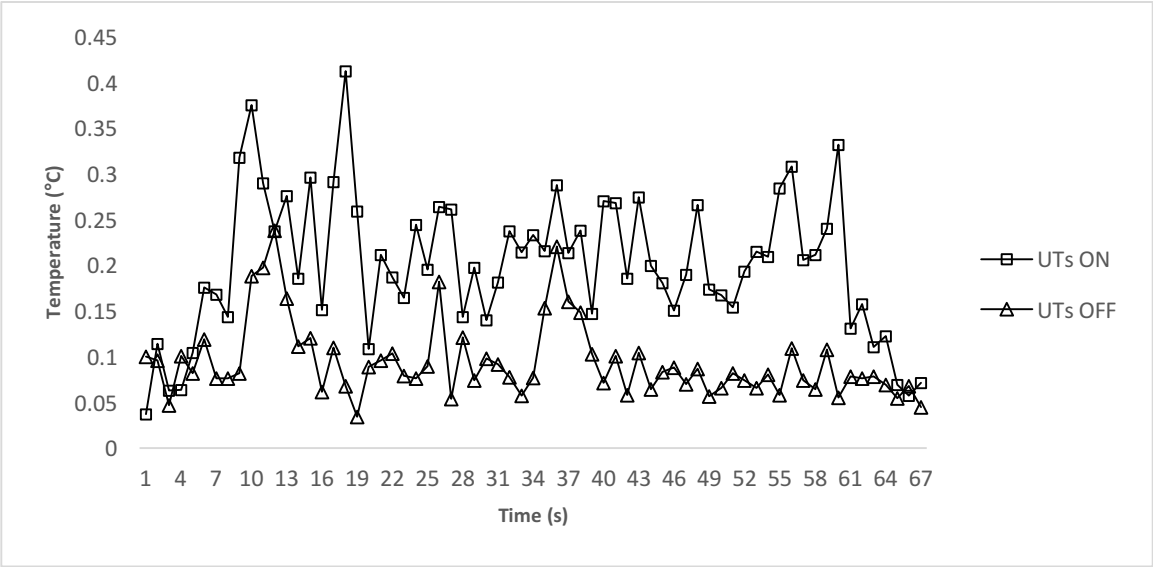


Figure 15 400 ml/min: DTC dT/dt

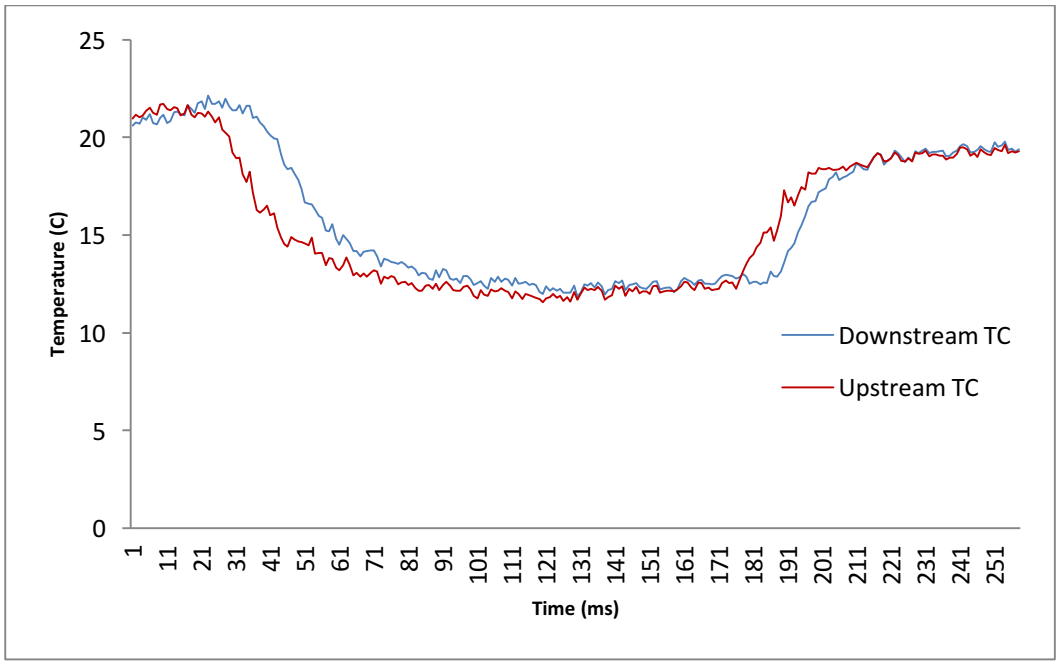


Figure 16 650 ml/min: Temperature Data UTs On

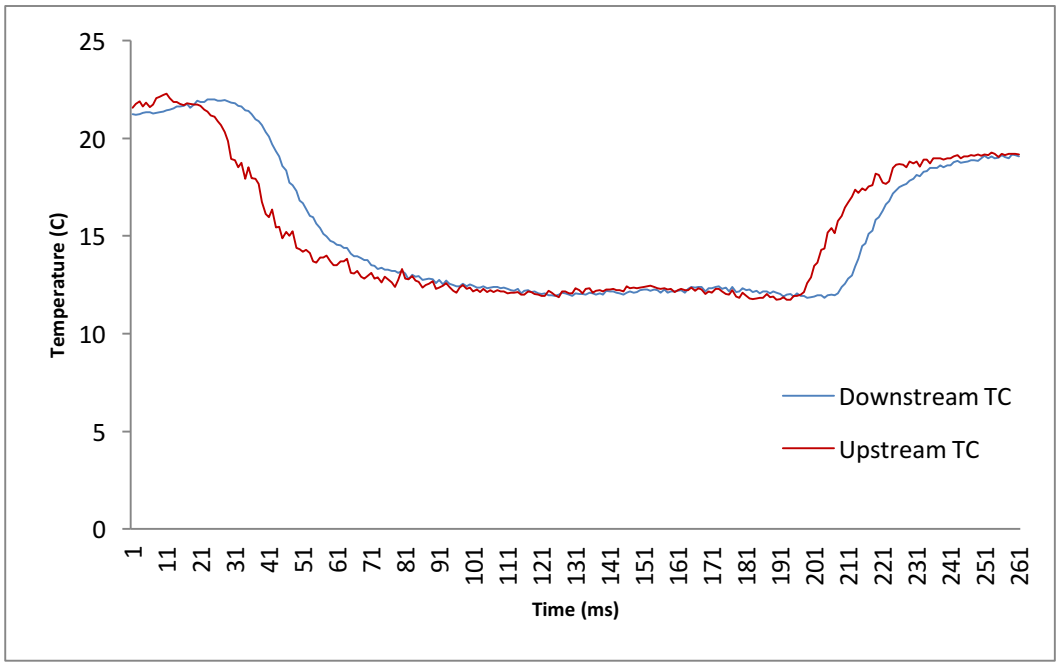


Figure 17 650 ml/min: Temperature Data UTs Off

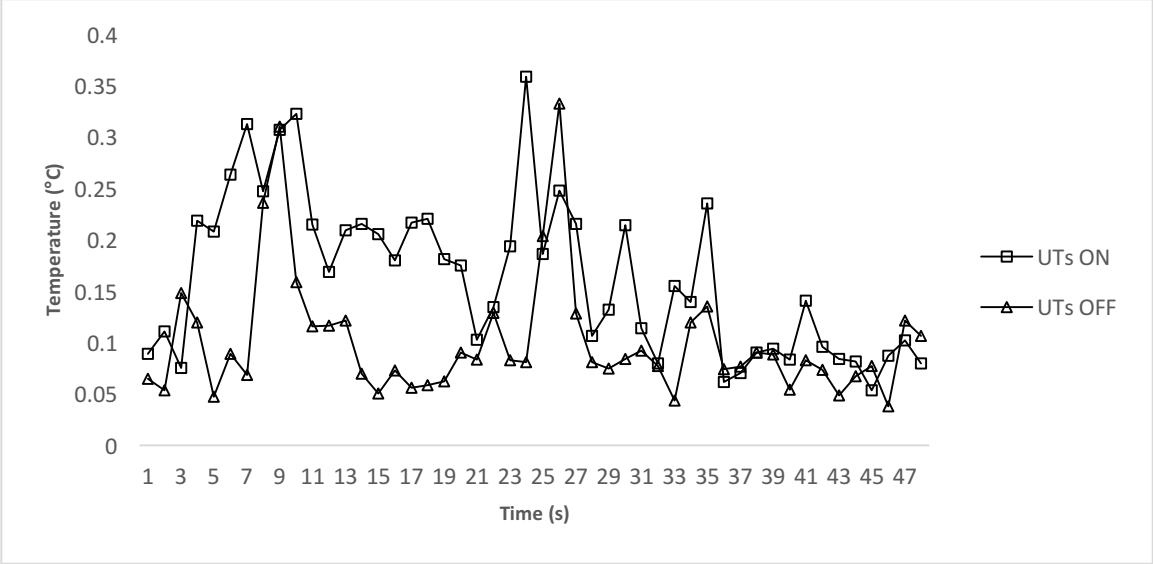


Figure 18 650 ml/min: DTC dT/dt

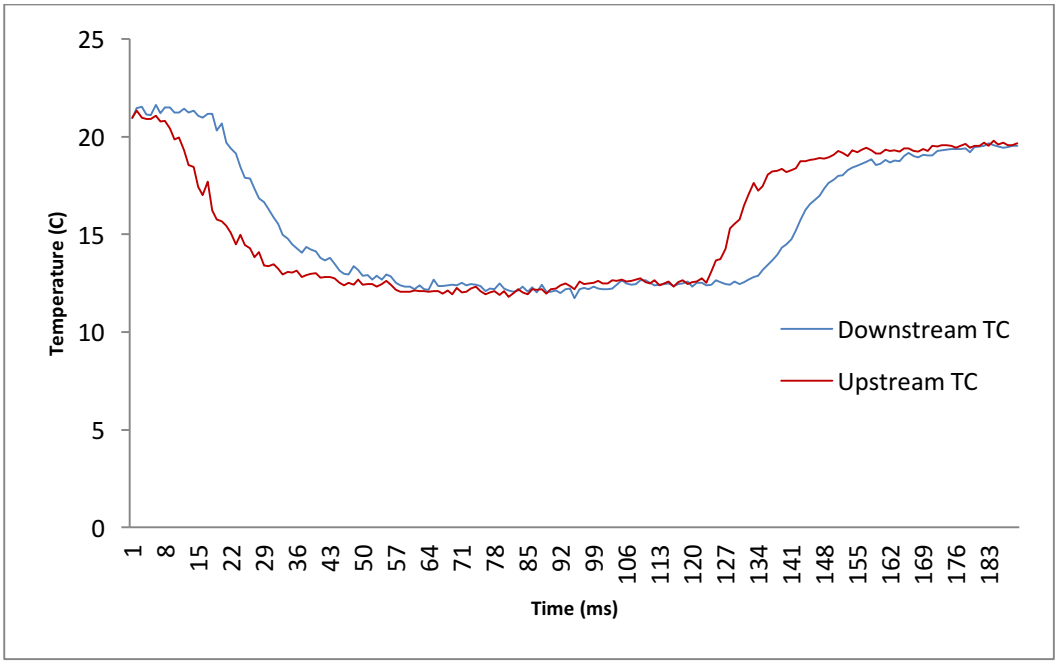


Figure 19 1200 ml/min: Temperature Data UTs On

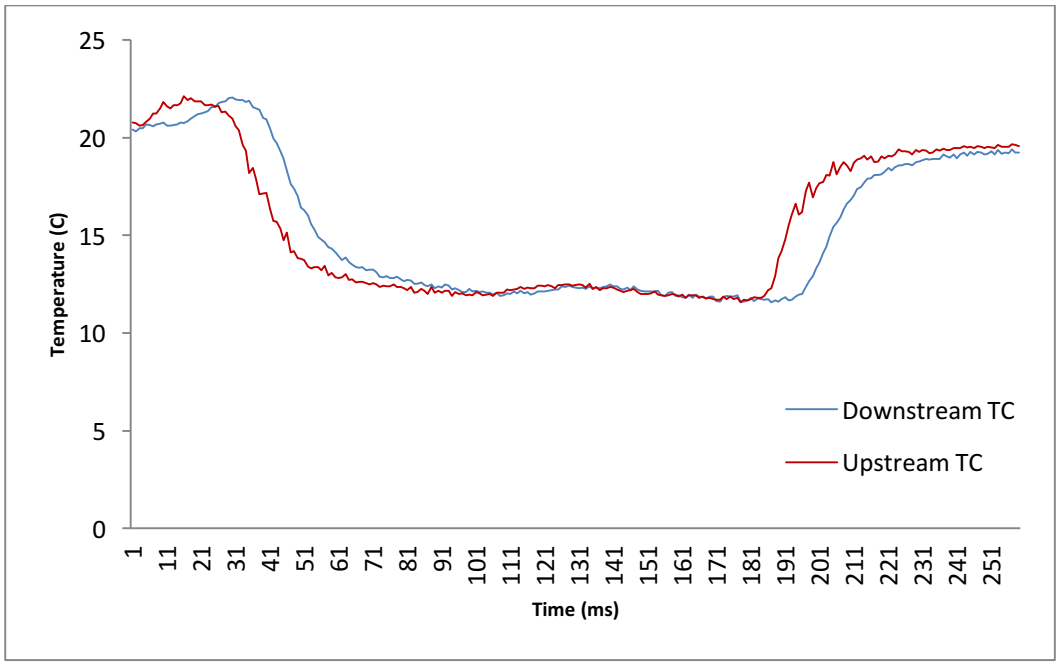


Figure 20 1200 ml/min: Temperature Data UTs Off

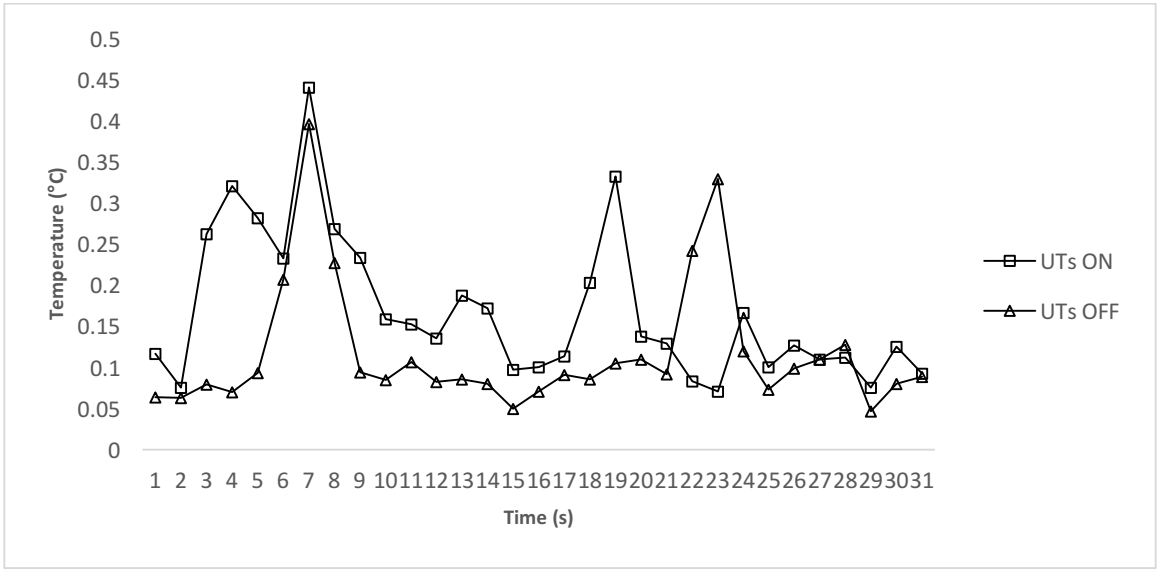


Figure 21 1200 ml/min: dT/dt

Peristaltic pumps are positive displacement pumps which use flexible tubing to carry the fluid. The rollers contained in the front housing compress the flexible tubing creating occlusions. The distance between each roller determines the volume of liquid moved in each pulse. As the driveshaft rotates, each of the rollers displace fluid causing a natural pulsation in the flow. At low speeds, the pulsations do not cause a noticeable change in the thermocouple data, however, as can be seen in the following pressure graphs, the higher flow rates exhibited large pressure fluctuations. These fluctuations were responsible for the noise in the thermocouple data and were addressed in future design iterations.

The data contained in figures 22-25 demonstrates the pressure fluctuations caused by the peristaltic pump. At flow rate 1, the pressure pulses are low at approximately 2.5 psi. For flow rates 2 and 3, the pressure fluctuations are more significant at 6 and 12 psi, respectively. Flow rate 4 exhibits the greatest pressure change with fluctuations over 17 psi.

As can be seen from the thermocouple data provided above, the ultrasonic transducers had a significant impact on the heat transfer rate. Although the data is positive, several design issues had to be address before the data could be considered reliable. Specifically, the pressure fluctuations had to be resolved as well as the time required for the upstream thermocouple to reach the cold bath temperature. As can be seen in all the figures showing both the cooling and heating phases, for example Figure 19, the upstream temperature does not immediately change to the cold bath temperature.

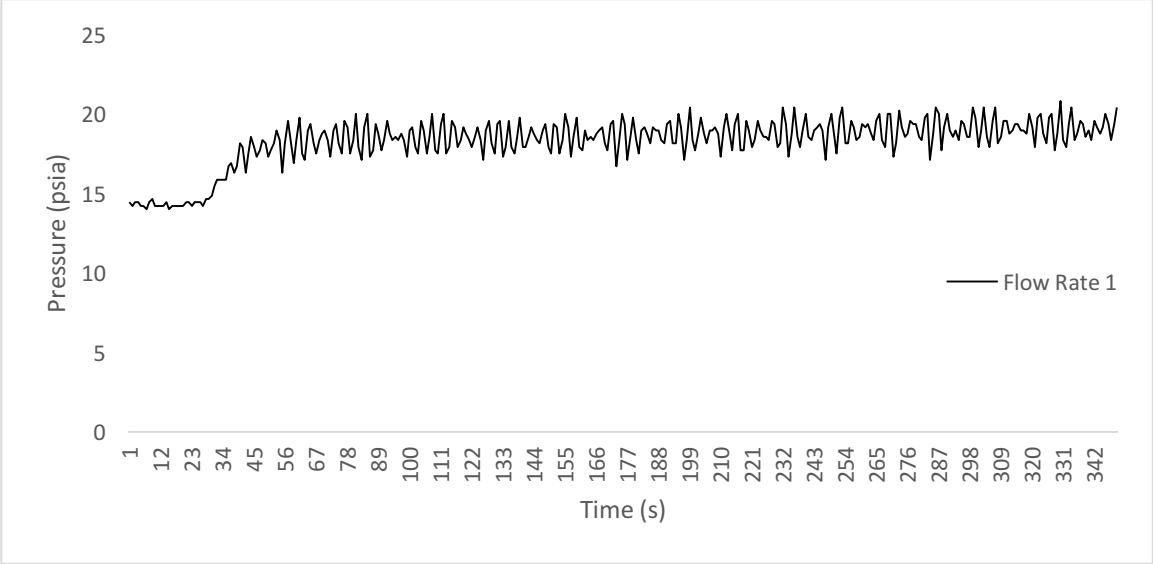


Figure 22 Pressure Data Flow Rate 1

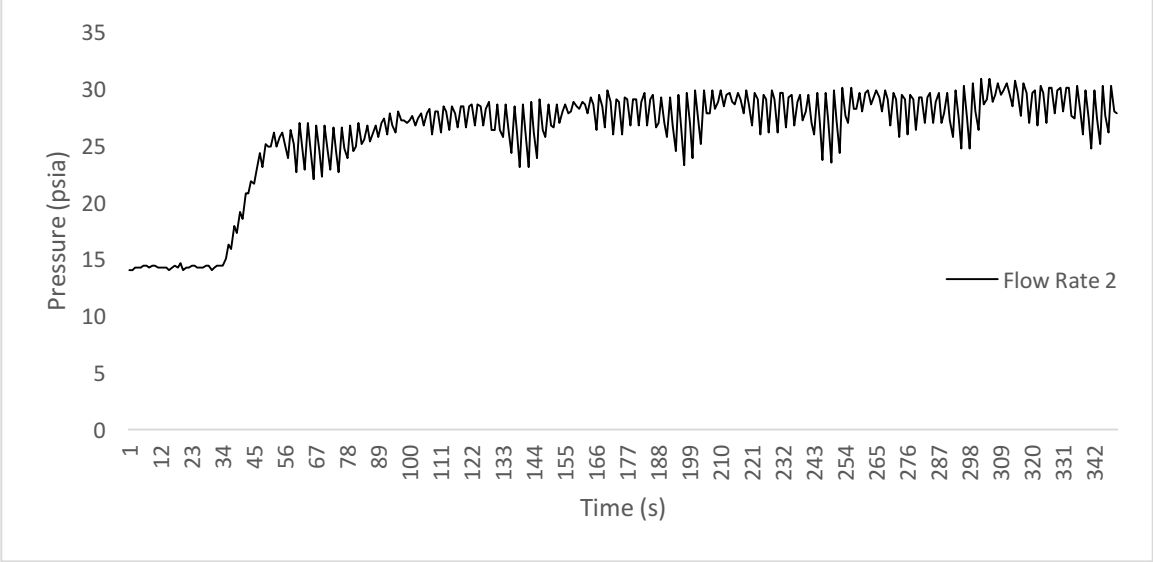


Figure 23 Pressure Data Flow Rate 2

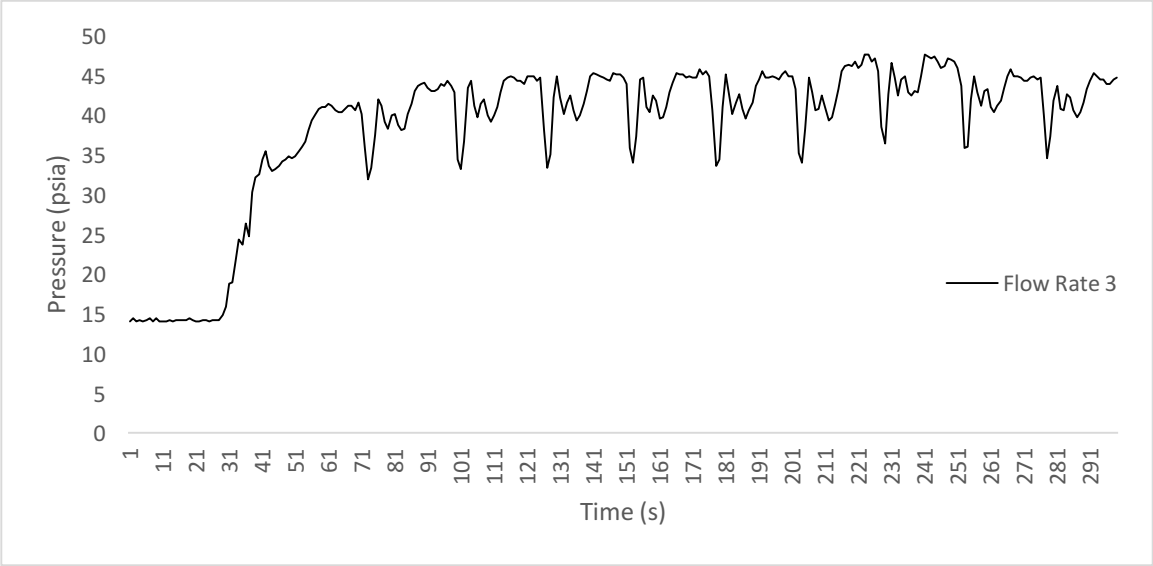


Figure 24 Pressure Data Flow Rate 3

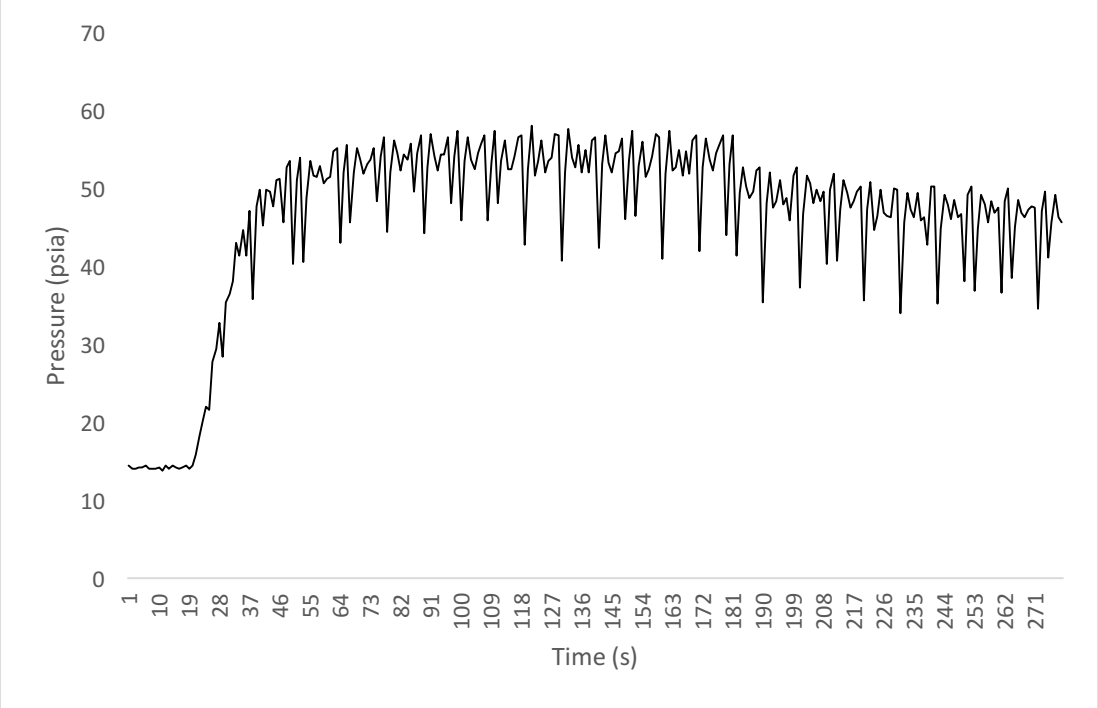


Figure 25 Pressure Data Flow Rate 4

In fact, the lowest temperature reached is 20% warmer than the cold bath temperature. The difference in the lowest temperature reached and the cold bath temperature is likely a function of heat loss along the tubing and heat generation where the pump rollers contact the flexible tubing.

Additionally, the upstream temperature transition was delayed due to the fact the cold water does not directly enter the inlet of the PPB. Instead, the cold water mixes with the warm water before the pump until all of the warm water is expelled. This mixing decreases the overall temperature experienced by the packed bed and requires the warm water to be processed first. The next chapter covers design alterations to address the above-mentioned issues and the related test results.

CHAPTER 5: PPB DESIGN WITH DAMPENER (4TH SETUP)

The two most significant issues from 0 testing were the pressure fluctuations caused by the peristaltic pump and heat loss upstream of the PPB. In order to address these issues, several design alterations were considered. First, the number of rollers on the peristaltic pump could be increased, however, the existing system used four rollers with a maximum of six possible. Although increasing the number of rollers would decrease the occluded volumes of fluid, and result in a more stabilized flow, the improvement would not satisfy the pressure requirements. Other pump styles were not available and design changes were required to utilize the peristaltic pump. Instead, it was determined that a dampener could be used to absorb the pressure fluctuations and would provide adequate results.

Considering the difference in the temperature shown directly upstream of the PPB versus the temperature of the cold bath, three design changes were made; removal of all metal valves, a redesigned plastic PPB and the addition of tube insulation. These design changes were expected to decrease heat loss between the cold bath and PPB and improve the overall test results.

Methods and Materials

As in previous tests, pressure readings were collected utilizing an Omegadyne pressure transducer with a pressure range of 0-200 psia and an output voltage of 0-5V.

A Synthware reflux condenser was used in series with a Lauda Brinkmann EcoLine Re106 chiller which provided a glycol coolant used to maintain a 10°C cold water bath for testing. The cold bath was connected to the pump via a plastic shut-off valve.

A Lab Glass bubbler was used downstream of the pump as an accumulator to reduce pressure fluctuations.

The ultrasonic transducers were powered by a T&C Conversion AG series amplifier which provided a sinusoidal voltage of approximately 28 volts at a frequency of 135 kHz. The amplifier was set to not exceed 2 watts.

Data Collection

Data from the pressure transducer was collected via a National Instruments NI9201 module with a voltage accuracy of .015 volts and sampling rate of 500 kS/s. Analog thermocouple readings were collected utilizing a National Instruments 9213 module with 50Hz/60Hz noise rejection and up to .02 °C temperature sensitivity. All data was process using LabVIEW with a sampling rate of 10 Hz. Figure 26 provides a schematic of the system design with the integrated dampener.

Experimental Procedure

Testing began by initiating data collection via LabVIEW at which point the peristaltic pump was turned on with the warm bath valve open and the cold bath valve closed. Warm fluid was passed until the entire system reached thermal

equilibrium as indicated by equal readings of the upstream and downstream thermocouples.

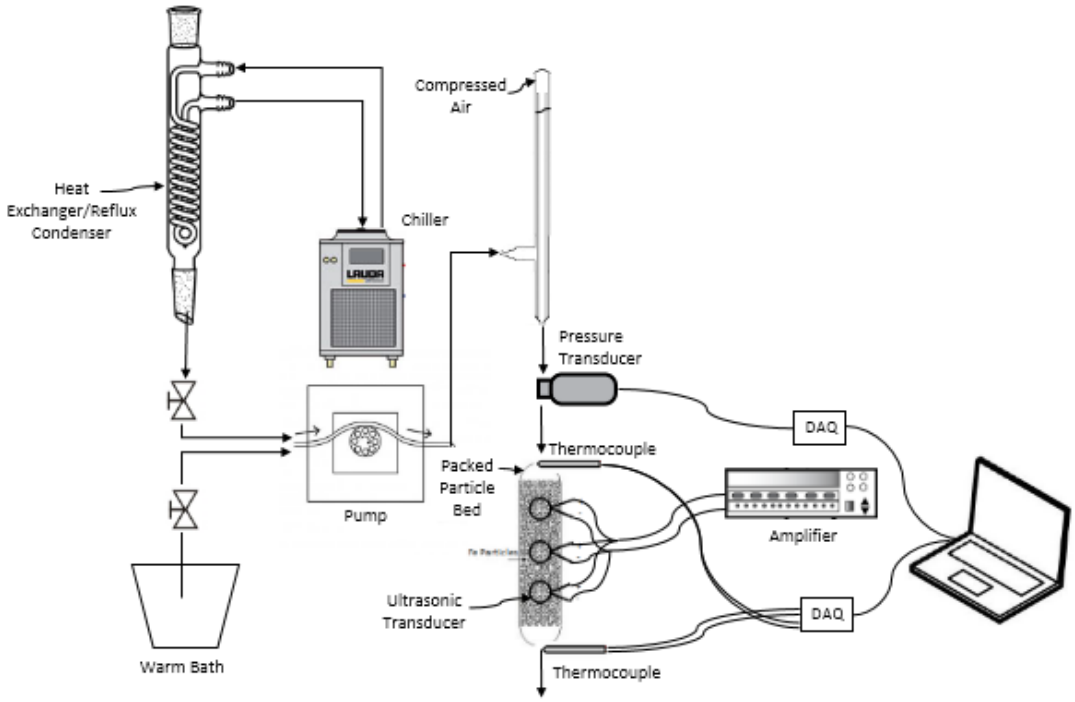


Figure 26 PPB Design with Dampener

During the heating phase, the dampener slowly filled reaching an equilibrium pressure dependent on the flow rate. Once a pressure and temperature steady-state was reached, the warm bath valve was closed and the cold bath valve was opened. This allowed the 10°C water to pass through the system and cool the PPB. The test time was limited by the cold bath tank size and was dependent on the associated flow rate. At higher flow rates the system was unable to reach as cold of a temperature as with slower flow rates due to the

limited cold bath volume. Data was written to files for analysis. Fresh water was added at the end of each test and allowed to cool to 10°C prior to each subsequent test. Data was also collected during warm-up cycles immediately following the cool-down cycle. This allowed for two sets of heat transfer data per test. The above methods were repeated at each flow rate.

Results and Discussion

Initial testing focused on evaluating the effects of the dampener on the pressure fluctuations. Although the system experienced an approximate 65% decrease in pressure variance, the dampener introduced other significant problems. Specifically, once the pump was energized, the water first passed through the dampener which required a substantial period of time before it was filled and reached a stabilized pressure. This resulted in a variable flow rate experienced by the PPB during each test. As can be seen in figures 27 and 28, the pressure stability was greatly improved with the use of a dampener. However, the red circle in Figure 28 represents the period during which the dampener cylinder was building pressure. Once the dampener was filled, the pressure stabilized and a relatively stable flow was established. Figure 28 also shows a 54 second delay between the initialization of the tests and the point the system pressure stabilizes.

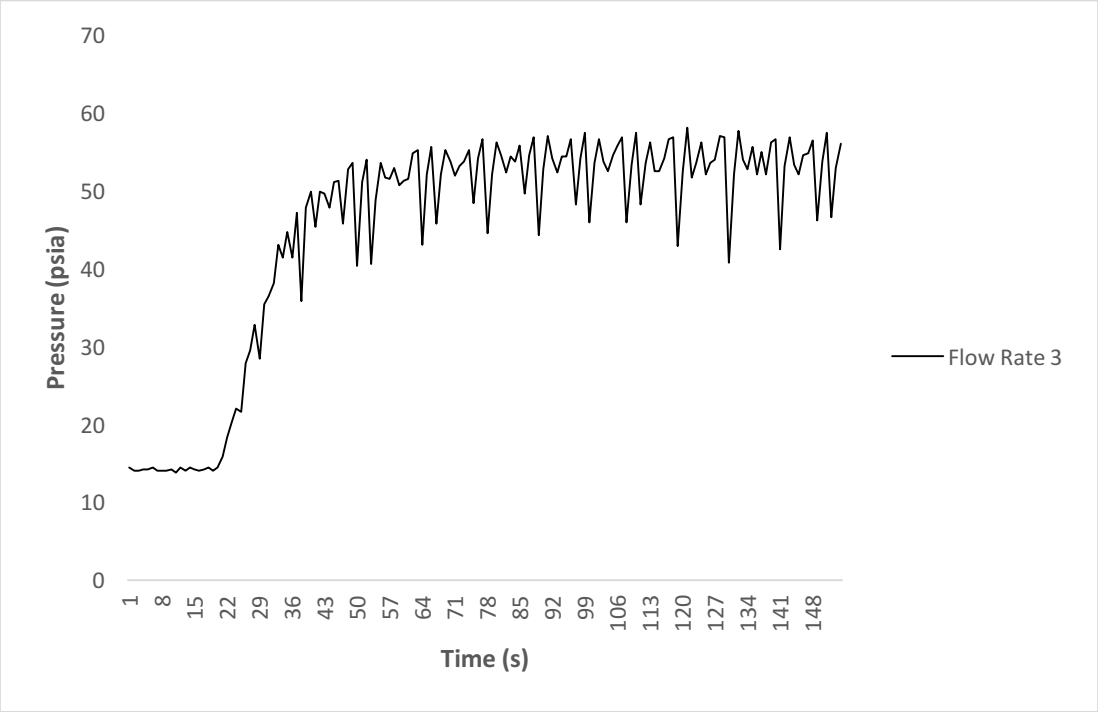


Figure 27 Pressure Fluctuations without Dampener

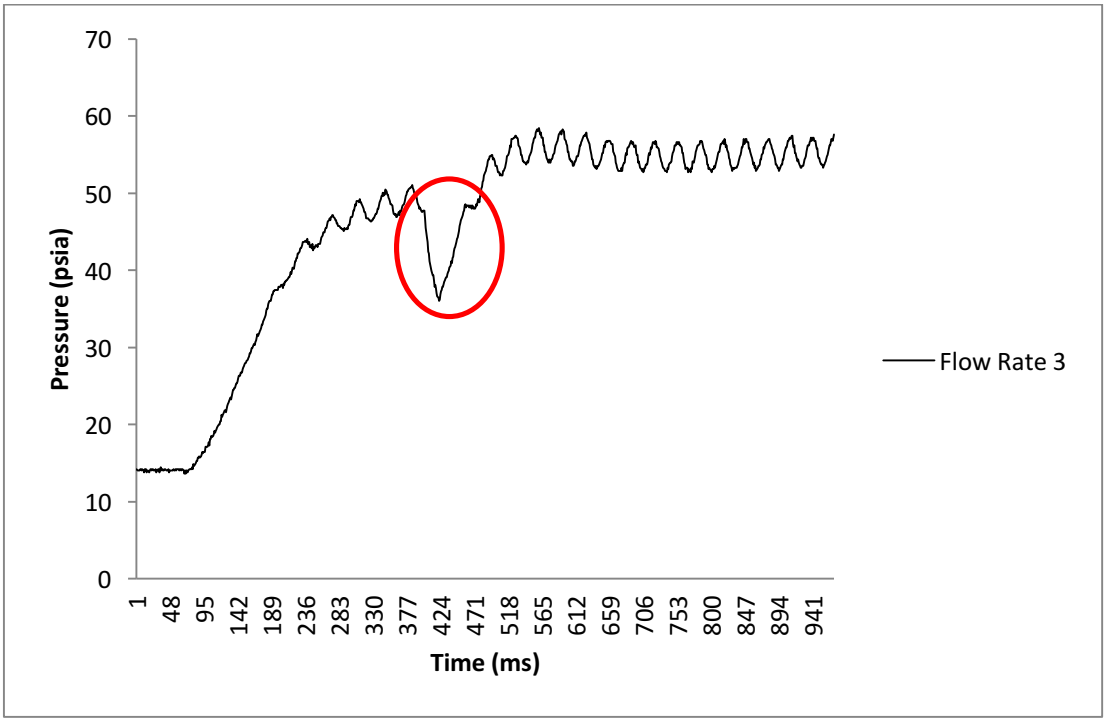


Figure 28 Pressure Fluctuations with Dampener

Other complications occurred as a result of using the dampener. Specifically, the warm and cold water was forced to mix during both cool-down and warm-up test. For example, following cool-down tests, the dampener was filled with cold water and the entire system was at the cold bath temperature. The warm-up tests were then initiated by passing the warm bath fluid through the system and into the PPB. During this time, the cold fluid mixed with the warm liquid until the cold water was completely displaced. This mixing yielded temperature results that were unsatisfactory. Figure 29 shows an example of the temperature curves during a warm-up test. The upstream thermocouple slowly received the warm water as the dampener filled until the pressure stabilized and the flow rate was steady. To produce consistent and reliable data, the mixing of fluids and the pressure issues had to be resolved.

Isolation Valve

In order to avoid additional delays due to a system-wide redesign, a slight modification to the dampener was used. The warm and cold water mixing, as well as the delay in reaching a stabilized pressure, were addressed using an isolation valve integrated directly upstream of the PPB. This valve was initially closed, while the dampener reached a stable pressure, and then was opened to initiate the tests.

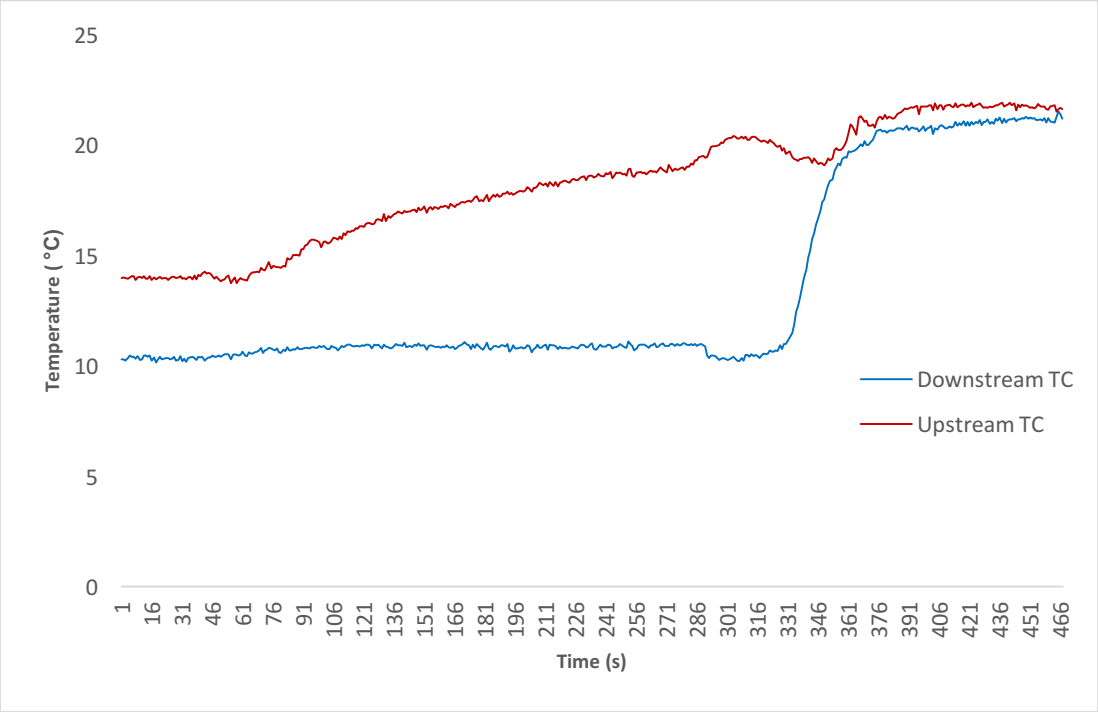


Figure 29 Warm-up Temperature Curves with Dampener

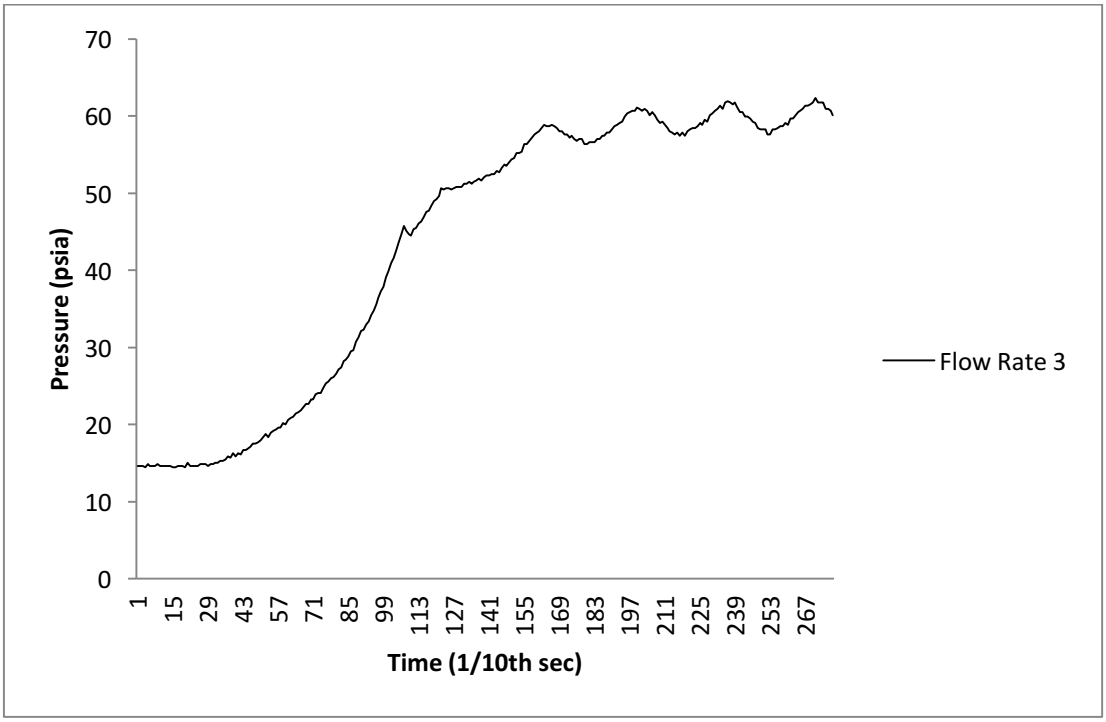


Figure 30 Pressure Data with Isolation Valve

The results from tests utilizing the isolation valve are not explored in their entirety as good data was not produced, however, the following figures show improvements in both temperature and pressure data at a flow rate of 650 ml/min. The use of the isolation valve allowed the system to reach a stable pressure approximately 65% faster. This improvement, although significant, was not sufficient and did not yield reliable data. Figure 31 provides an example of the temperature data collected during the experiments utilizing the isolation valve.

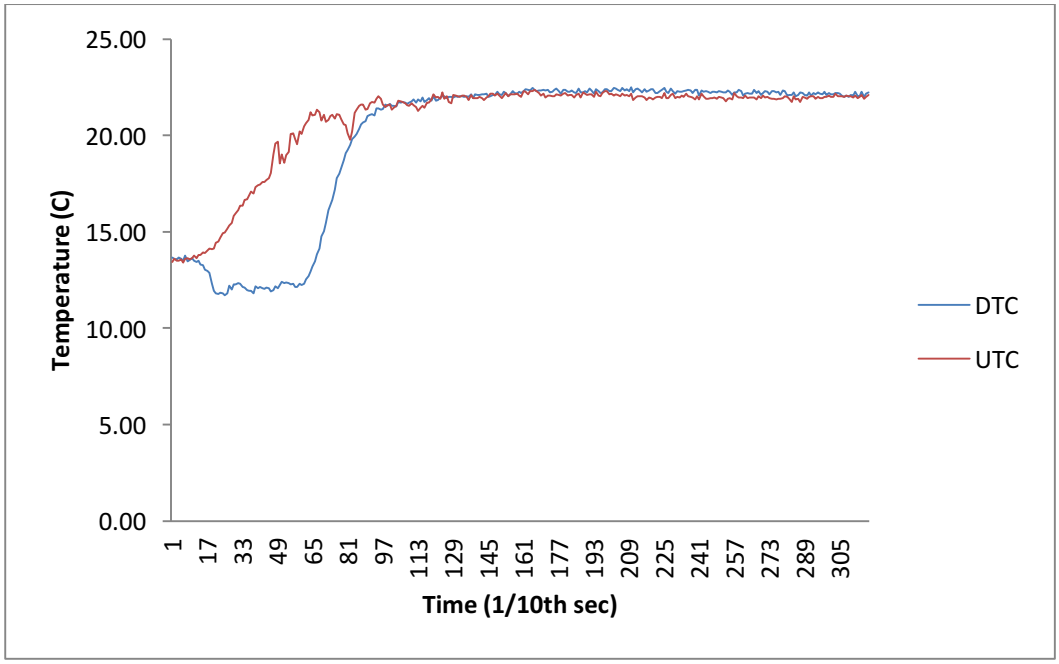


Figure 31 Temperature Data with Isolation Valve

When compared with the data from Figure 29, the upstream thermocouple experiences a much faster temperature change. Although the upstream temperature change was not rapid enough, it represented a 74% improvement.

The data in Figure 31 also confirmed the pressure fluctuations continued to cause undesirable fluctuations in the temperature.

With the primary goals being a highly stable flow and the ability to introduce both warm and cold water directly to the PPB inlet, further design changes were required.

CHAPTER 6: FINAL DESIGN (5TH SETUP)

In the final design iteration, significant improvements were made. In previous system designs, the intent was to utilize existing resources to determine if the use of ultrasonic transducers would significantly improve heat transfer in packed particle beds. Although early testing required numerous design changes, the data collected indicated the UTs provided noteworthy improvements to heat transfer. Consequently, additional resources were made available, upgrading system components and improving the quantity and quality of data collected. Specifically, a flow controller was purchased as well as other materials which made it possible to utilize a unique valve system. The flow controller allowed for the accurate monitoring and control of high pressure water sources. The valve system made it possible to not only establish a system-wide temperature equilibrium, but also inject the warm and cold bath fluids immediately upstream or downstream of the PPB. This valve system, insured the PPB would experience a rapid change in fluid temperature either upstream or downstream, depending on the testing procedure. The following sections discuss the results collected using the final system design.

Materials and Methods

As in previous tests, pressure readings were collected utilizing an Omegadyne pressure transducer with a pressure range of 0-200 psia and an output voltage of 0-5V.

In order to insure the cold bath volume was sufficient to perform extended testing, a 25-liter cooler was used as the cold bath vessel. A helical coil heat exchanger was fabricated from aluminum tubing with a 6.5 mm O.D. and 4.5 mm I.D. Two separate coils were wound with diameters of 51 mm and 102 mm from one consecutive tube length. The 51 mm tube was integrated axially with the 102 mm section for a total tube length of 6.6 meters. The flow rates chosen insured the heat exchanger would sufficiently cool the process water to the 2 °C cold bath temperature. The cold bath vessel was filled with a mixture of water and ice and a temperature of approximately 1.5-2 °C was maintained throughout all tests.

An Alicat LCR liquid flow controller capable of controlling flow rates up to 5 liters per minute was connected to lab water at a pressure of 71 psig and 22 °C. The flow controller output was connected to a three-way valve in order to direct flow either through the heat exchanger during cool-down tests, or through the downstream side of the PPB to return the system to room temperature. The proportional-integral-derivative (PID) settings were adjusted for each flow rate to minimize oscillations.

Modified three-way valves were integrated upstream and downstream of the PPB in order to allow fluid to flow through the system in either an upstream-to-downstream direction or reverse. Additionally, the valves allowed for the isolation of the PPB from the system while all tubing and valves reached either the cold or warm bath temperature. This system minimized heat loss and

reduced test-cycle time. The valves were placed immediately above and below the PPB in order to insure the fluid would enter the system directly.

The ultrasonic transducers were powered by a T&C Conversion AG series amplifier which provided a sinusoidal voltage of approximately 28 volts at a frequency of 135 kHz. The amplifier was set to not exceed 2 watts.

Data Collection

Data from the pressure transducer was collected via a National Instruments NI9201 module with a voltage accuracy of .015 volts and sampling rate of 500 kS/s. Analog thermocouple readings were collected utilizing a National Instruments 9213 module with 50Hz/60Hz noise rejection and up to .02 °C temperature sensitivity. All data was process using LabVIEW with a sampling rate of 10 Hz.

Particle Selection

Corrosion of the iron particles in previous tests caused permanent changes in porosity, permeability and the pressure drop across the PPB. If iron particles were continued to be used, the entire PPB would need to be rebuilt after each tests. In order to eliminate this design flaw, stainless steel particles were used. The particles were purchased from Alfa Aesar with an estimated particle size of -40 to 80 mesh. The elemental composition, along with the associated weight fraction is outlined below. The particle size distribution was determined

using sieves with varied meshes. Table 4 provides the particle distribution data for 100 grams of stainless steel particles.

Table 4 Stainless Steel Particle Distribution

Mesh Size (μm)	**Mass (g)**
300	15.6
250	43.4
212	24.7
180	14.5
150	1.3
125	.4
106	.1

Given the distribution of particle size found in Table 4, the Sauter mean diameter, d_{32}, was calculated as follows:

$$D_i = \sqrt[2]{Ui * Li} \quad (1)$$

where U_i and L_i are the upper and lower limits of each sieve size and D_i is the geometric mean. Next, D_i was used with the weight fraction, ϑ_i, to calculate d_{32}:

$$D[3,2] = \frac{\sum_i^n Di^3 * \vartheta i}{\sum_i^n Di^2 * \vartheta i} \quad (2)$$

$$d_{32} = 270.13\ \mu m \quad (3)$$

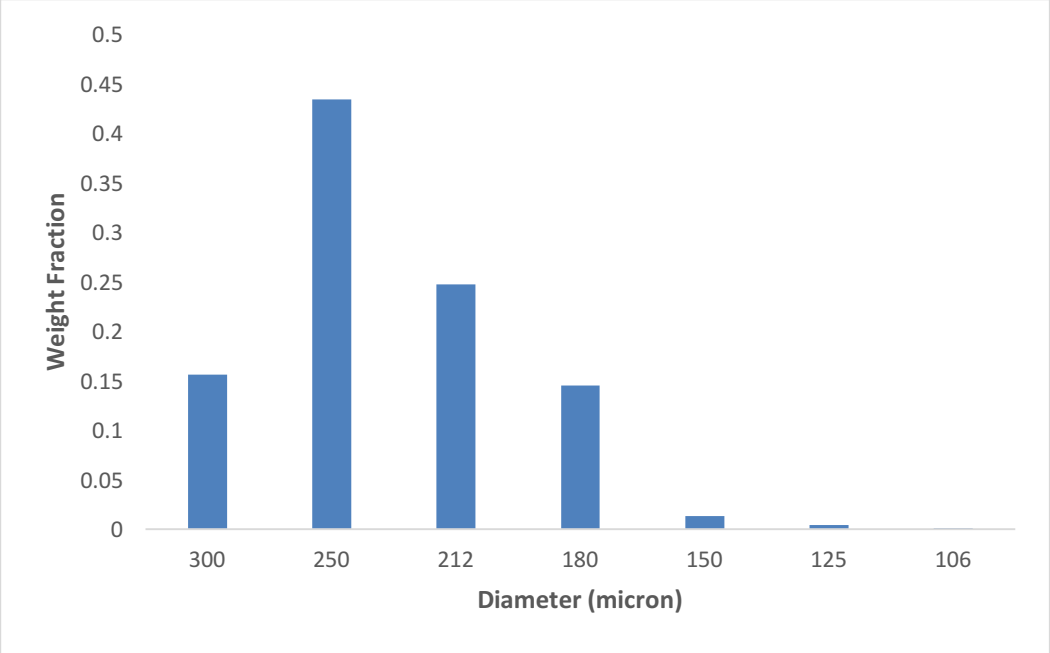


Figure 32 Particle Size Distribution

The PPB void fraction, ε, was calculated using the mass of the particles, M_p, the volume of the bed,V, and the density of the particles,ρ_p, as follows:

$$\varepsilon = 1 - \frac{M_p}{V\rho_p} \quad (4)$$

$$\varepsilon = .453 \quad (5)$$

The density of the stainless steel particles was calculated according to Table 5.

Table 5 Particle Density Data

	% of Total	Density	Partial Density
Fe	0.675	7850	5298.75
Cr	0.17	7190	1222.3
Ni	0.13	8909	1158.17
Mo	0.025	10188	254.7
		Total Density	**7933.92**

Pressure Drop

There are numerous methods to calculate the pressure drop across packed particle beds, however, the most common utilizes the Ergun equation. Equation (6) is suitable for a wide range of conditions including laminar and turbulent flow. The equation also accounts for variances in particle characteristics including non-spherical particles as is the case in this study:

$$\frac{(-\Delta p)}{H} = 150\frac{\mu U}{x_{sv}^2}\frac{(1-\varepsilon)^2}{\varepsilon^3} + 1.75\frac{\rho_f U^2}{x_{sv}}\frac{(1-\varepsilon)}{\varepsilon^3} \tag{6}$$

where $\frac{\Delta p}{H}$ is the pressure drop per unit length, μ the dynamic viscosity, ρ_f the fluid density, ε the void fraction, U the superficial velocity and x_{sv} the Sauter mean diameter. The modified Reynolds number was calculated as follows:

$$Re_p = \frac{\rho U x_{sv}}{\mu(1-\varepsilon)} \tag{7}$$

where U is calculated using equation (8)

$$U = \frac{Q}{A} \tag{8}$$

and Q is the volumetric velocity and A is the cross-sectional area of the packed particle bed.

Packed particle beds can experience undesirable near-wall effects if the tube-to-particle diameter, $\frac{Dc}{dp}$, is not controlled. For low Reynolds numbers <10, and a low tube-to-particle diameter, the pressure drop can be significantly altered due to wall effects which is not accounted for in the Ergun equation. A modification to the Ergun equation developed by (Reichelt) was used to determine if the particle size selected would affect the pressure drop near-wall. The friction factor, f_p, was derived from the Ergun equation using the modified Reynolds number as follows:

$$f_p = \frac{150}{Re_p} + 1.75 \tag{9}$$

However, equation (9) does not take into account the tube-to-particle diameter. The following modifies the Ergun friction factor:

$$f_p = \frac{150M^2}{Re_p} + \frac{M}{B} \tag{10}$$

where, M and B are defined as,

$$M = 1 + [\frac{2}{3} * \frac{1}{(1-\varepsilon)} * \frac{d_p}{D_c}] \quad (11)$$

$$B = [1.15\left(\frac{d_p}{D_c}\right)^2 + .87]^2 \quad (12)$$

Time Constant

Considering the system behavior in terms of the time domain, it can be represented as a simple first-order step function of the form,

$$m\dot{v} + cv = f \quad (13)$$

which has no input derivative and can be converted to the following form using the Laplace transform:

$$v(t) = v(0)e^{\frac{-ct}{m}} + \frac{F}{c}(1 - e^{\frac{-ct}{m}}) \quad (14)$$

where v(t) is the summation of the free and forced responses, v(0) is the initial state of the system at t=0, c and m are constants, and F is the magnitude of the step input. In order to compare the heat transfer data collected via experimentation, (14) was expressed in terms of the time constant, τ, where,

$$\tau = \frac{m}{c} \quad (15)$$

which represents the amount of time required for the system to decay to 37% of the value at t=0. The time constant dictates the rate of change of the system. To further simplify equation (14), the steady-state condition, v_{ss}, is defined as,

$$v_{ss} = \frac{F}{c} \tag{16}$$

such that equation (14) can be represented as,

$$v(t) = v(0)e^{\frac{-t}{\tau}} + v_{ss}(1 - e^{\frac{-t}{\tau}}) \tag{17}$$

The amount of energy required for the stainless steel particles to transition from room temperature to the cold bath temperature was used as the baseline for performance comparison. The specific heat, C_p, of the stainless steel particles, the mass, m_p, of the particles and the difference between the warm and cold bath temperatures were used to calculate the total energy required for the particles to reach the cold bath temperature as follows:

$$Q = m_p C_p (T_{ini} - T_{ss}) \tag{18}$$

where Q is the heat transfer, T_{ini} and T_{ss} represent the initial temperature and steady-state temperature respectively. The time required by each system to transfer 67% of the energy from equation (18) was determined from the experimental data and used as the time constant.

Experimental Procedure

Prior to data collection and initializing the flow controller, the valves were positioned to allow warm water to pass through the PPB until the upstream and downstream thermocouples reached equilibrium. At this point, the valves were repositioned to allow the warm water to pass through the heat exchanger and reach the desired cold bath temperature of 2°C. During this time, the PPB was isolated, remaining at 22°C, while the valves and tubing reach the cold-bath temperature. This was achieved by setting the valves to direct the cold water upstream of the PPB and out to the drain.

Once the upstream tubing and valves reached the cold-bath temperature, the data acquisition system was initiated and the valves were once again repositioned. The cold water then passed through the PPB while pressure and temperature data was collected.

Given that data collected in prior testing indicated optimal results were achieved at lower flow rates, three flow controller set points were used—200, 400 and 600 ml/min. Although the system design allowed for the collection of pressure and temperature data during both warm-up and cool-down cycles, data was collected for cool-down cycles only.

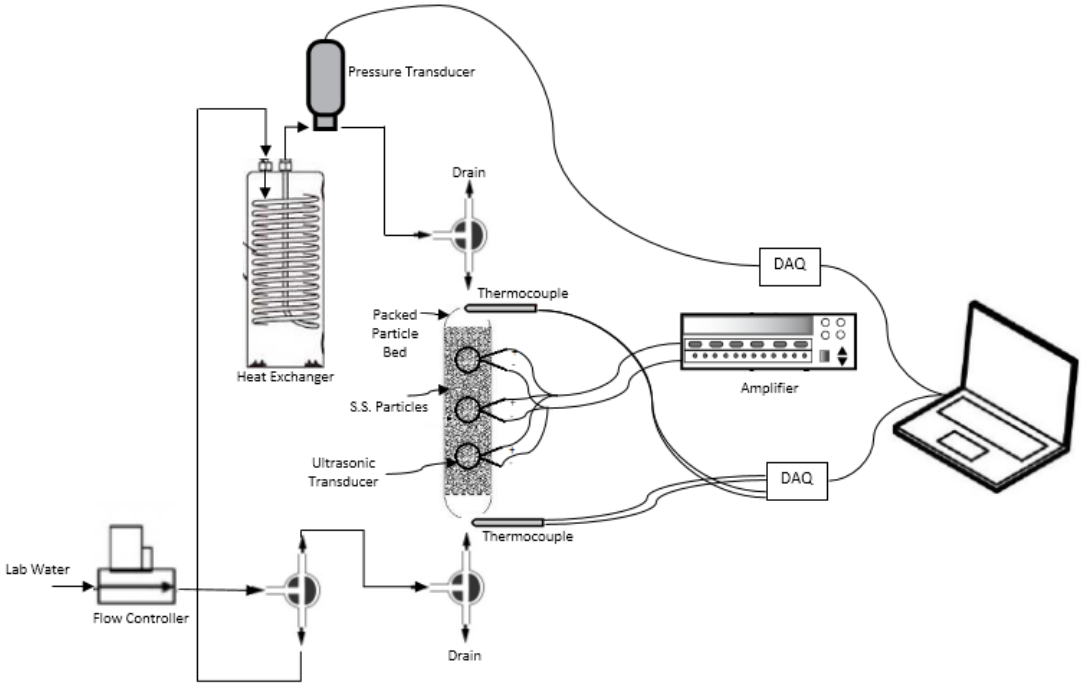


Figure 33 Final PPB Design

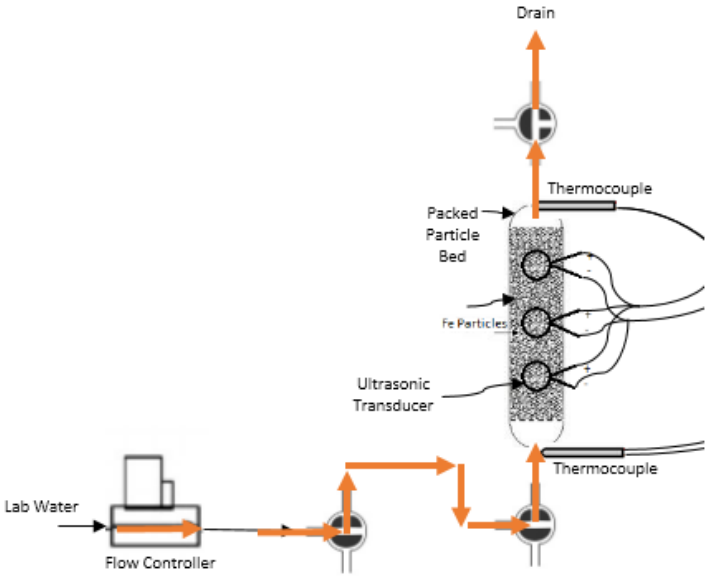


Figure 34 Flow Diagram: Warm-up cycle

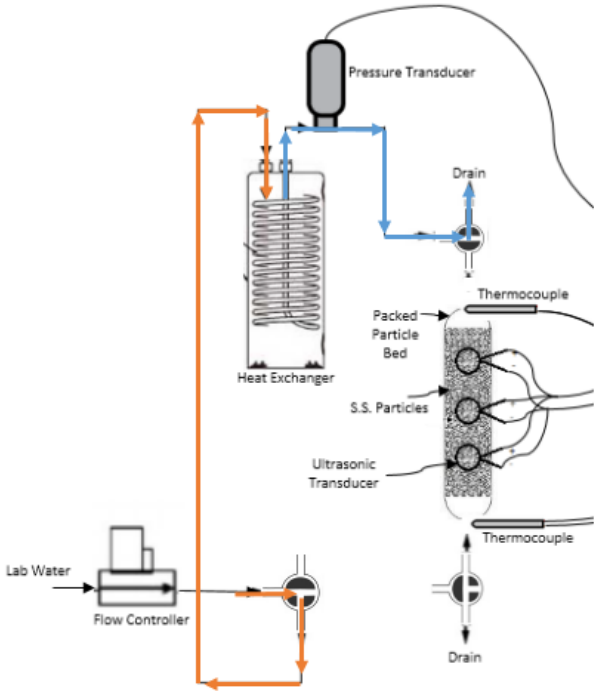


Figure 35 Flow Diagram: Initial cool-down cycle

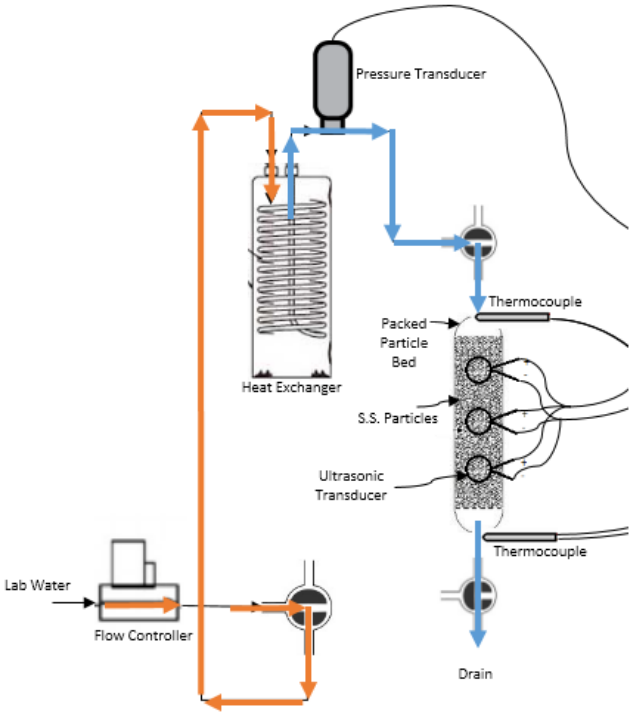


Figure 36 Flow Diagram: Cool-down testing

Results and Discussion

At both 200 ml/min and 400 ml/min, the system experienced improved heat transfer, however, as is supported in literature and was experienced in previous chapters testing, improvements were not present at the highest flow rate. At a flow rate of 600 ml/min, the two test cycles were similar, surprisingly however, the system without the UTs performed better.

The use of the flow controller eliminated the pressure fluctuations experienced in previous design iterations and provided a steady flow rate. The following figures highlight the pressure drop across the packed bed for tests with and without the UTs energized.

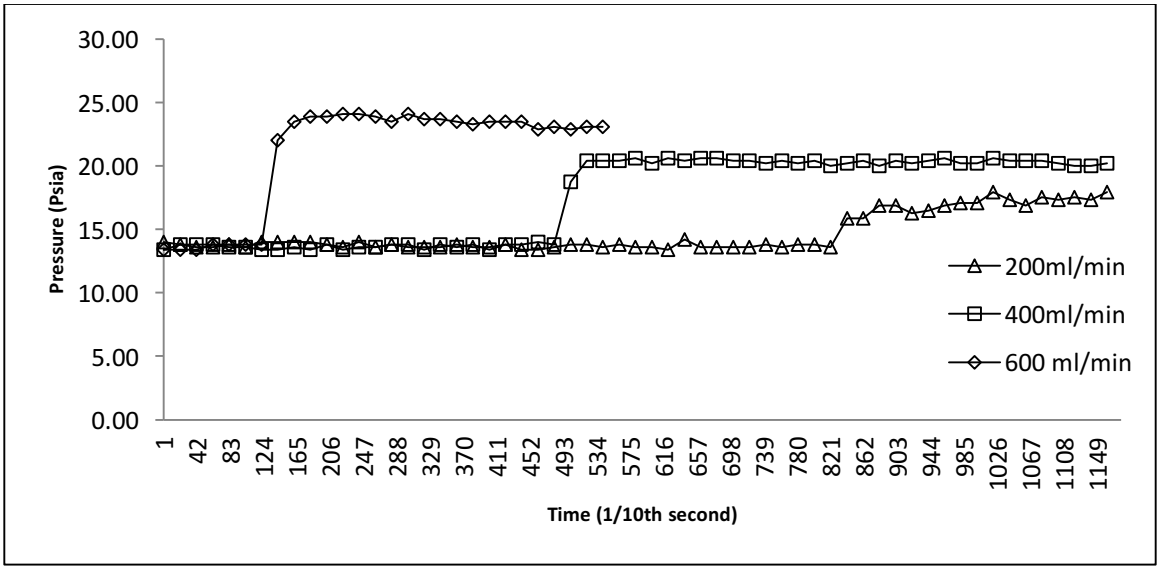


Figure 37 Pressure Drop with UTs OFF

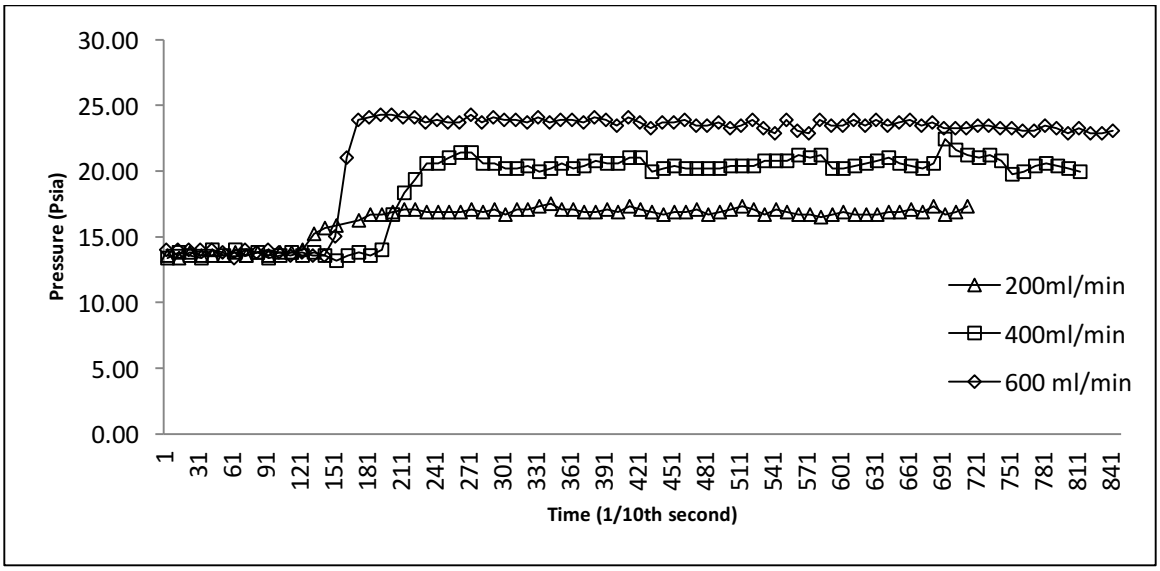


Figure 38 Pressure Drop with UTs ON

Although the effects were minimal, the oscillatory motion of the UTs while displacing the fluid caused small spikes in pressure. This is noticeable in the data set with the UTs energized.

Using equation (6), yielded the results in

Figure 39. The measured results were in close agreement with the predicted pressure drop using the Ergun equation and are tabulated in Table 6. The percent error can be found in Table 7. As was expected, the pressure readings while the ultrasonic transducers were turned off more accurately followed the predicted values. As mentioned before, the movement of the ultrasonic transducers displace the fluid within the packed bed and slightly alter the pressure drop.

Table 6 Pressure Data

	Pressure (Pa)		
Flow Rate (kg/s)	**UTs ON**	**Predicted**	**UTs OFF**
3.3E-06	16208.17	16463.85	15720.04
6.7E-06	42083.57	35892.38	38817.48
1.0E-05	64629.27	58285.58	60949.65

Table 7 Pressure Data Error

	Error	
Flow Rate (kg/s)	**UTs ON**	**UTs OFF**
3.3E-06	1.58%	4.73%
6.7E-06	-14.71%	-7.54%
1.0E-05	-9.82%	-4.37%

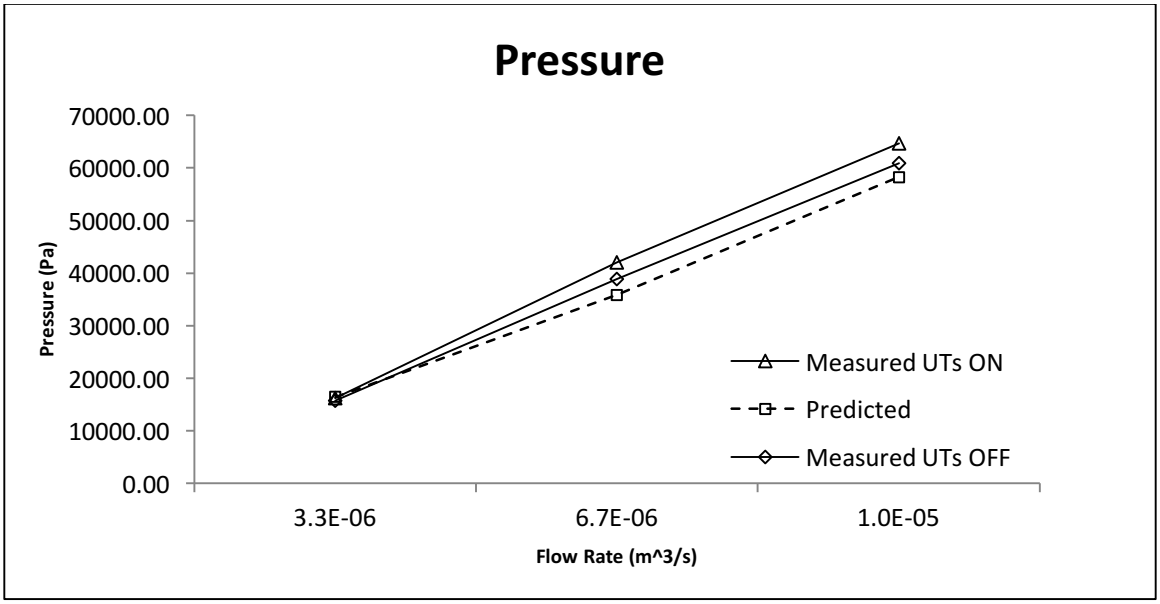


Figure 39 Pressure Drop Comparison Using Ergun Equation

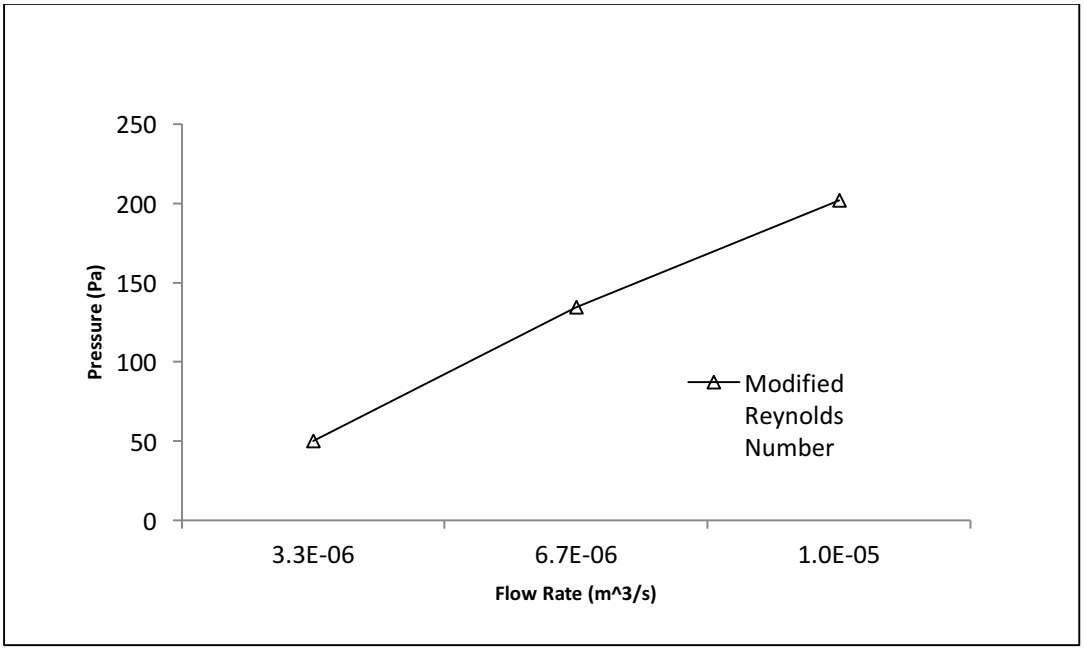


Figure 40 Modified Reynolds Number Data

Using equation (7) produced Reynolds numbers in the transitional range which indicated the Ergun equation was indeed a suitable choice where both the viscous and inertial effects contributed to the pressure drop. This study considered 3 different flow rates which generated modified Reynolds numbers of approximately 67, 135 and 202. The particle sizes used yielded a tube-to-particle ratio of approximately 50.

Using equations (10-12), Figure 41 was generated which confirms the impact of particle size on pressure drop in packed beds at low Reynolds numbers and low $\frac{Dc}{dp}$. Comparing the tube-to-particle diameter with the modified friction

factor also verified the particle size used in this study provided a sufficiently large tube-to-particle diameter ratio.

The first indication of improved heat transfer can be seen by considering the temperature profiles with and without the UTs. The downstream thermocouple data for the system with the UTs energized has a noticeably steeper slope. The difference between the downstream thermocouples (DTC) shows a significant improvement in the heat transfer process. The gap between the two curves indicates the DTC with the UTs energized converges toward the upstream temperature more rapidly than without the UTs. Although this visual comparison was useful in a preliminary sense, further exploration was required to quantify the differences at each flow rate.

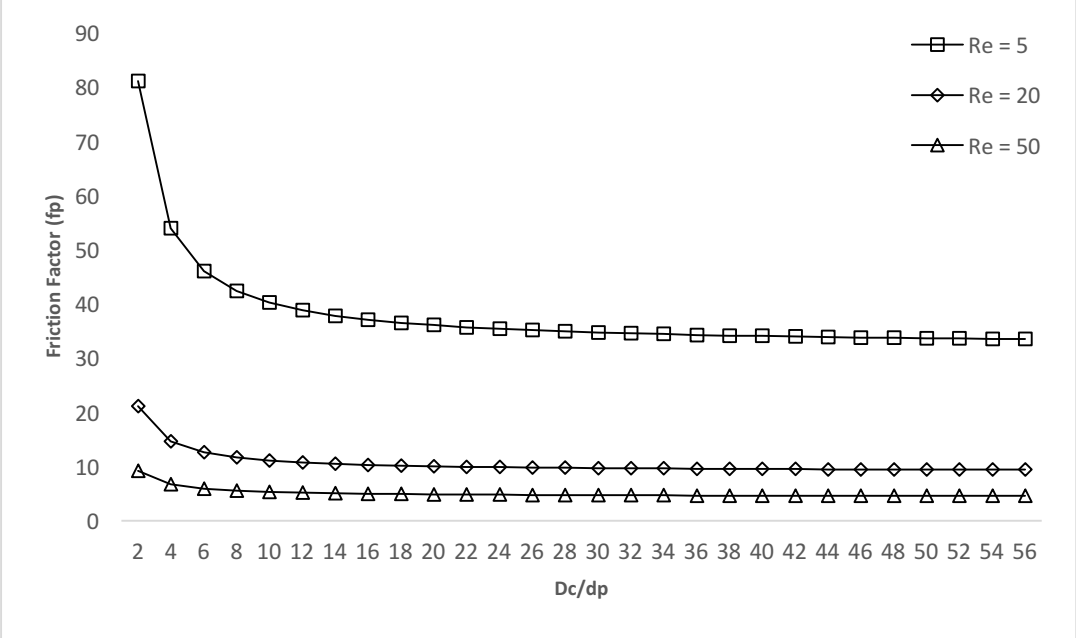


Figure 41 Friction Factor versus Tube-to-Particle Diameter

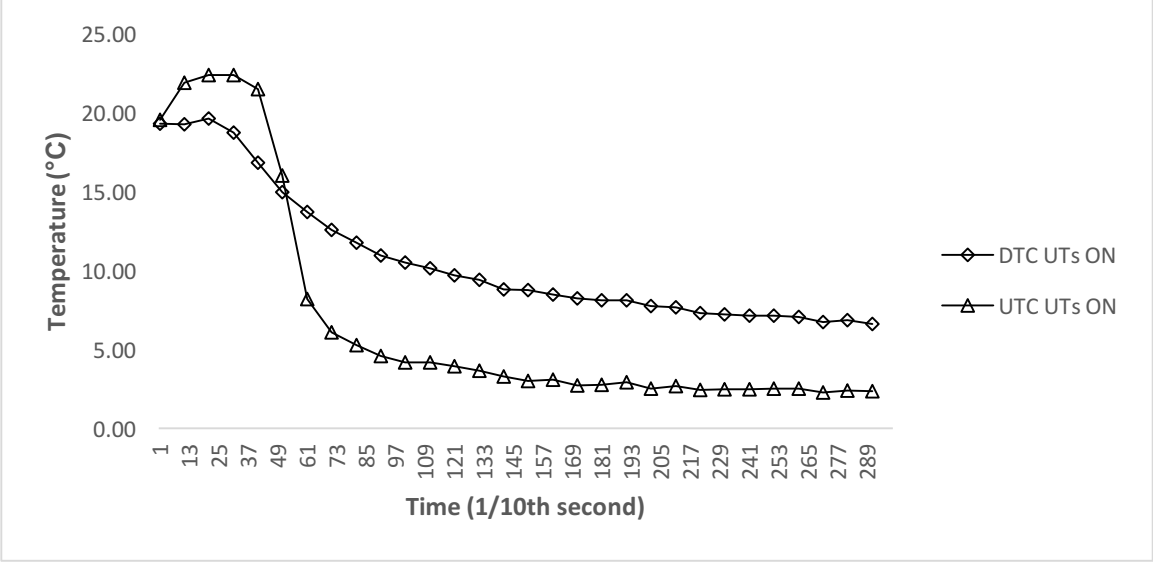


Figure 42 **200 ml/min:** Temperature Data with UTs Energized

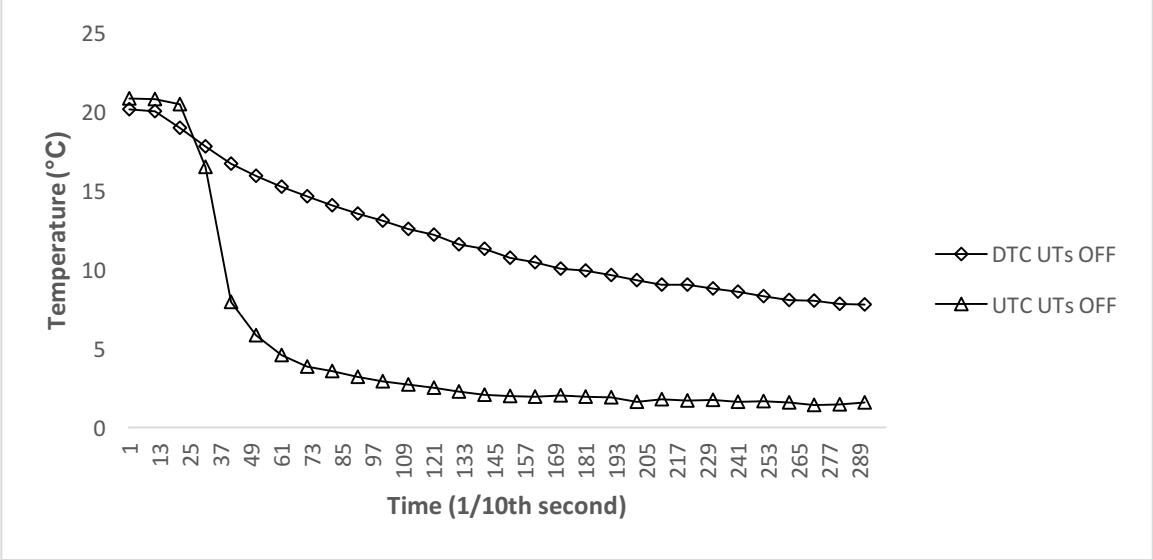


Figure 43 **200 ml/min:** Temperature Data without UTs Energized

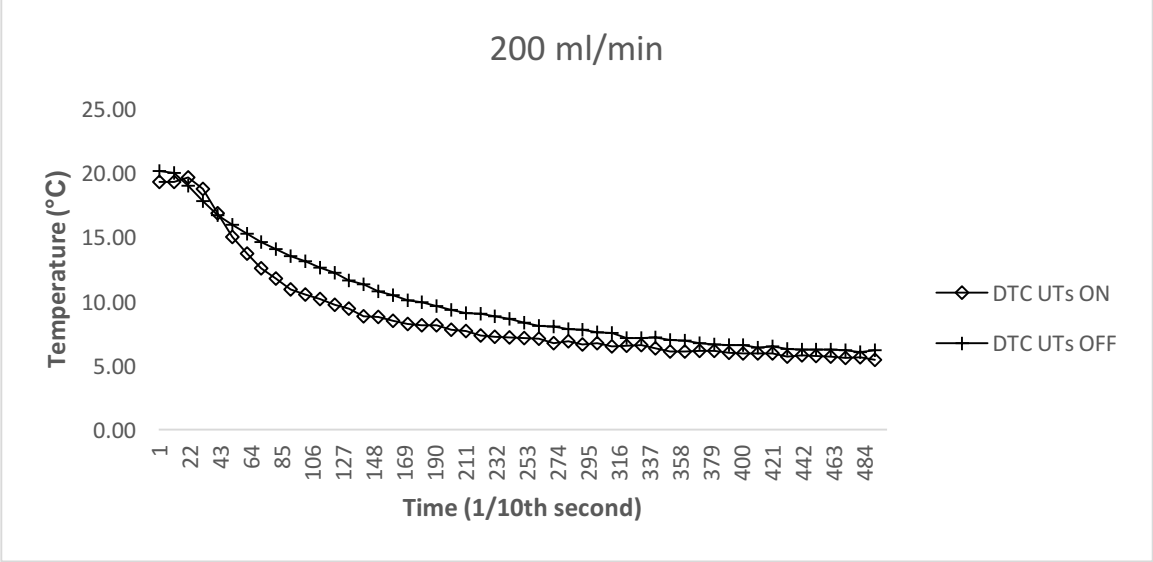


Figure 44 **200 ml/min:** DTC Comparison

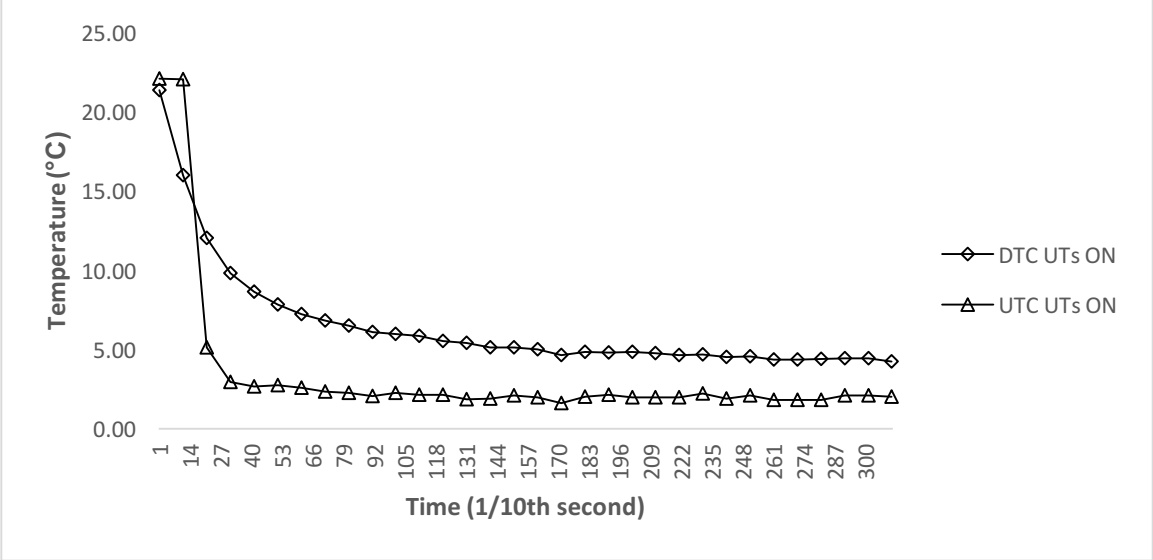


Figure 45 **400 ml/min:** Temperature Data with UTs Energized

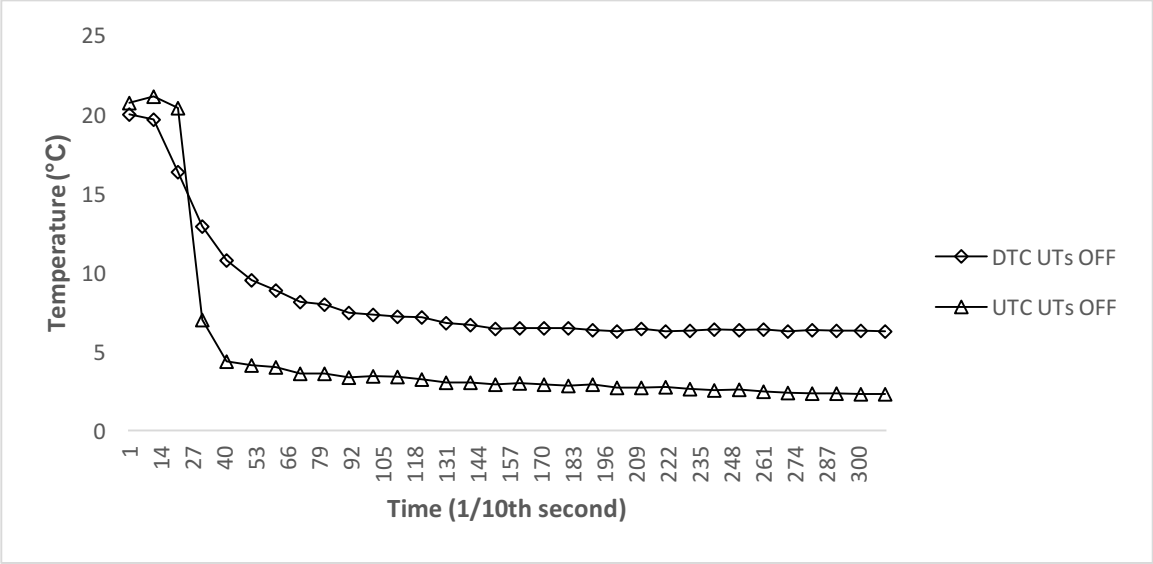


Figure 46 **400 ml/min:** Temperature Data without UTs Energized

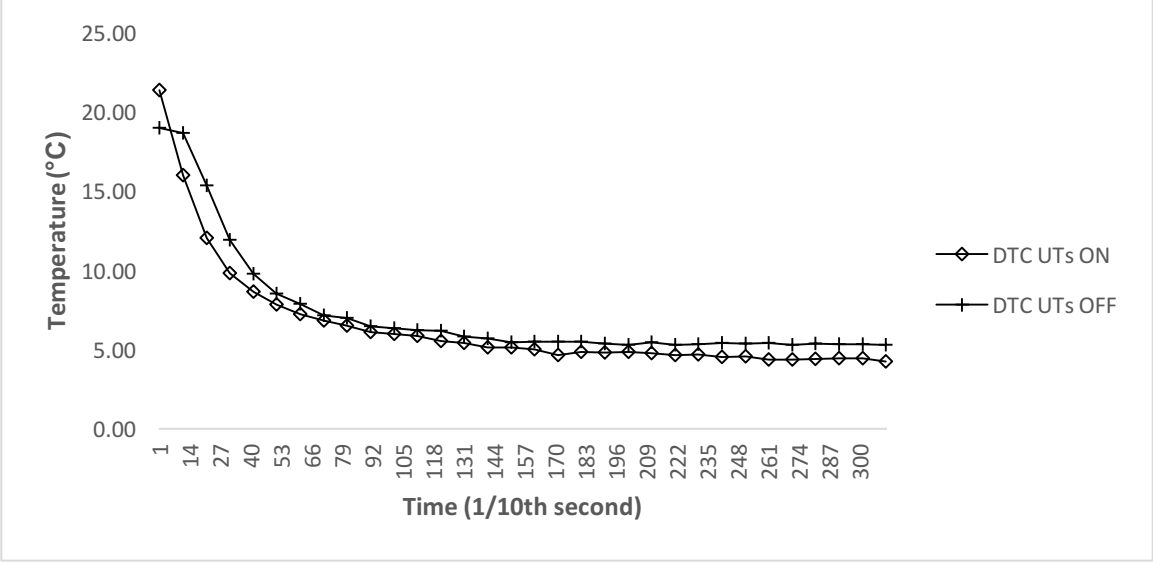


Figure 47 **400 ml/min:** DTC Comparison

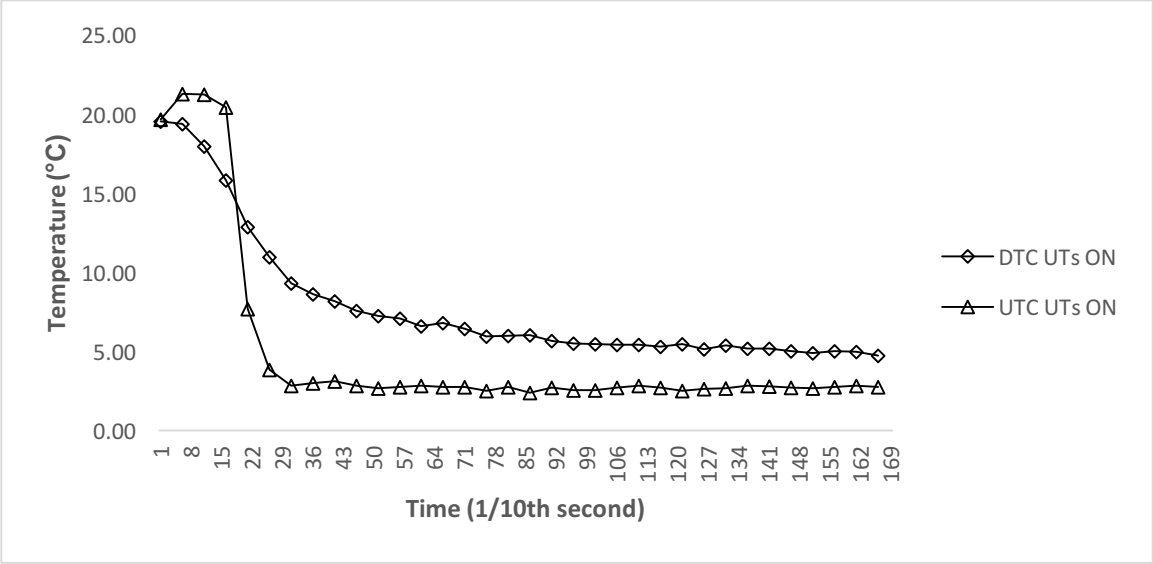


Figure 48 **600 ml/min:** Temperature Data with UTs Energized

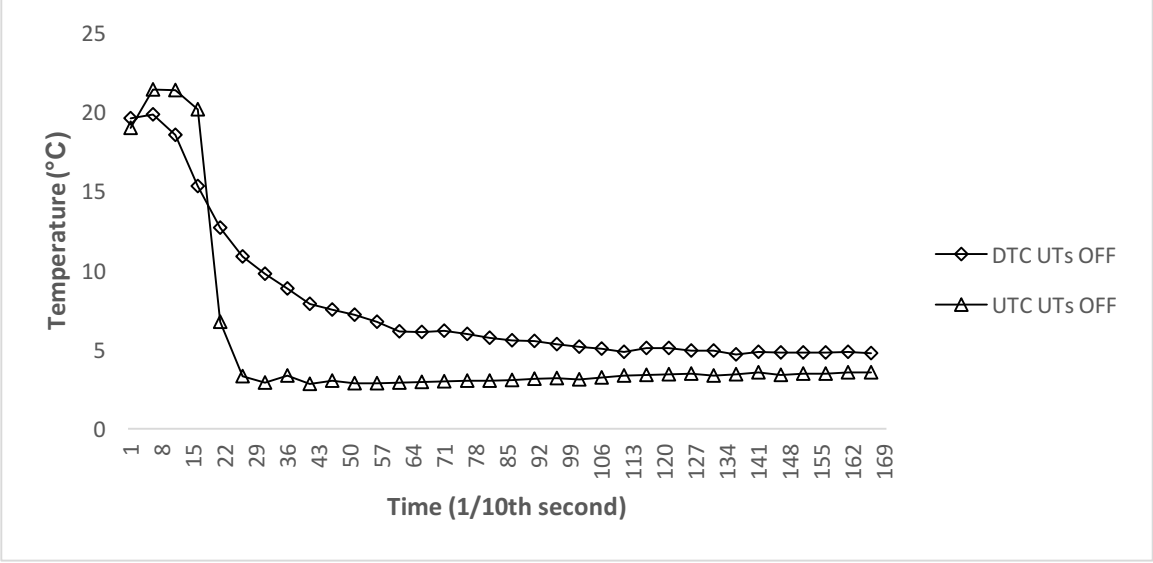


Figure 49 **600 ml/min:** Temperature Data without UTs Energized

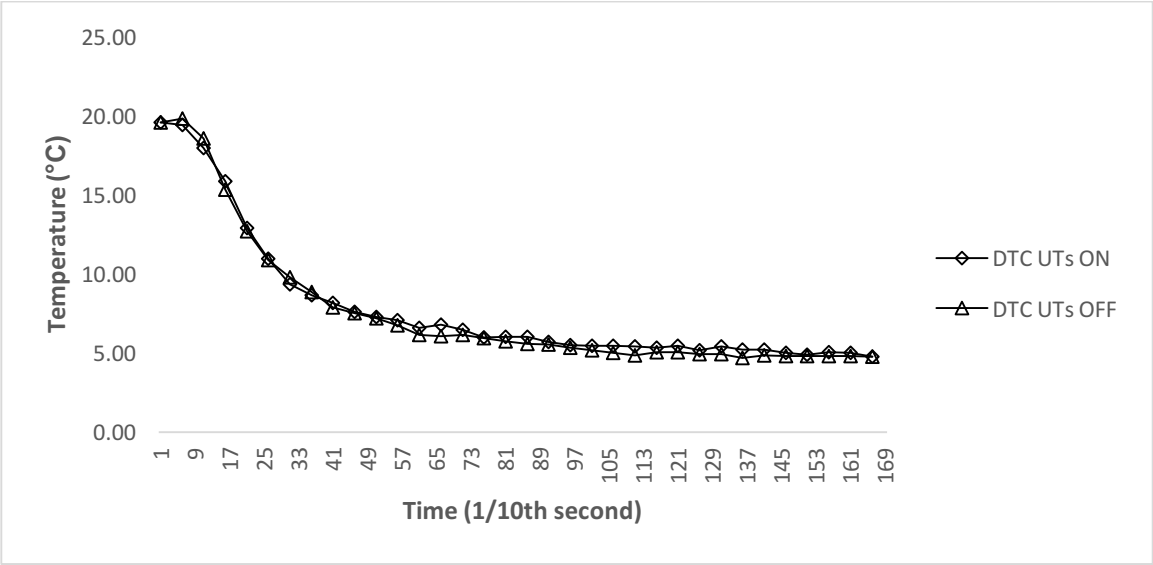


Figure 50 **600 ml/min:** DTC Comparison

Table 8 Time Constant Comparison

Flow Rate (m^3/s)	200 ml/min		400 ml/min		600 ml/min	
	UTs ON	**UTs OFF**	**UTs ON**	**UTs OFF**	**UTs ON**	**UTs OFF**
τ	63	104	24	42	4.8	5
% Difference	39%		43%		4%	

As both test cycles approach the same steady-state (cold bath temperature), a comparison of the time constants provided insight to which system exhibited the highest heat transfer rate. The optimum flow rate of 400 ml/min was determined by comparing the time constant data found in Table 8.

As was expected, the ultrasonic transducers improved the heat transfer rate. In keeping with literature, the improvements occurred at lower flow rates. It is hypothesized this is in part due to the ability of the ultrasonic transducers to displace fluid as a percentage of total axial flow. As the UTs oscillate, the fluid in contact with the surface is displaced in the radial direction. Many transducers are fabricated from one solid piece of ceramic, however, in this study transducers with a metal mesh center were used. The center mesh was fabricated to have decreasing diameter pores which allowed for capillary forces, combined with the direction of the disc movement, to create acoustic and mechanical streaming. The transducers were aligned so that the induced fluid streaming was focused in alternating radial directions. This design allowed for adjacent, radial fluid streams to more evenly disrupt the fluid flow along the length of the bed.

In comparison to packed bed systems without UTs, the design considered in this study allowed for the disruption of an otherwise laminar and fully developed flow. By integrating ultrasonic transducers into the packed bed, the system exhibited an increased turbulent flow without the associated pressure drop.

With a heat transfer rate improvement of over 40% and less than 2 watts total supplied to the transducers, this study is a significant departure from data in literature. All other studies use larger transducers with lower resonant frequencies that require significantly more power to operate. Even in studies where lower power was supplied, the input power was still over 15 times greater than the power used in this study. The system size and geometry likely contribute to power requirement variances, however, the most significant difference is the internal integration of the ultrasonic transducers.

To further verify the validity of the 1st order step function, a second comparison of the time constants for each system was made. In this comparison, the time required for the downstream thermocouple to transition from approximately 20 °C to 7.4°C, with the ultrasonic transducers turned on as well as off, was considered. This transition represented a 63% decrease in temperature as is required for a comparison of time constant. The following figures demonstrate close agreement between the 1st order step function and the experimental data for both systems.

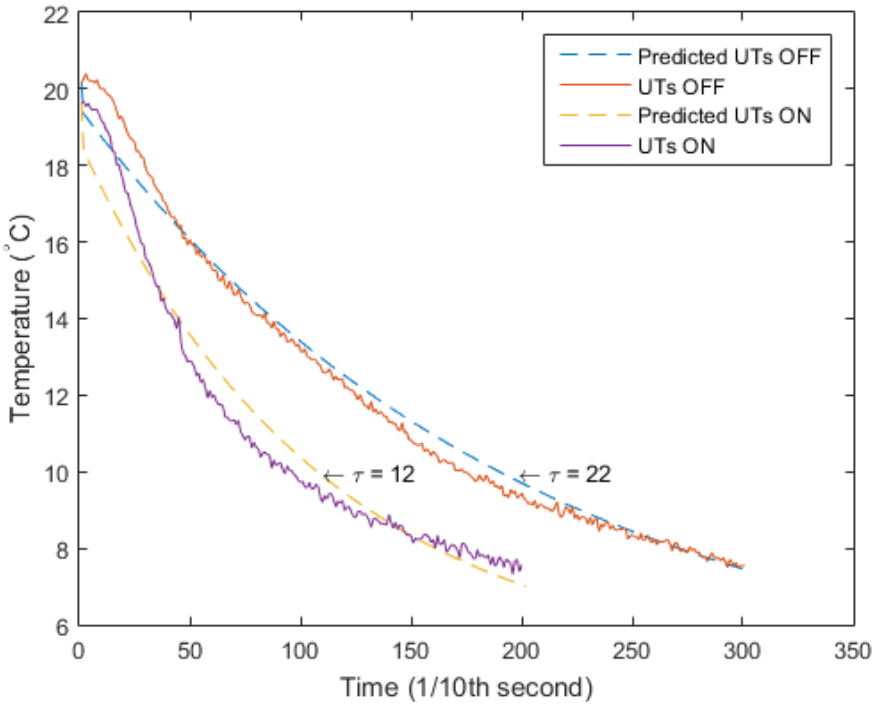


Figure 51 Temperature Time Constant Comparison

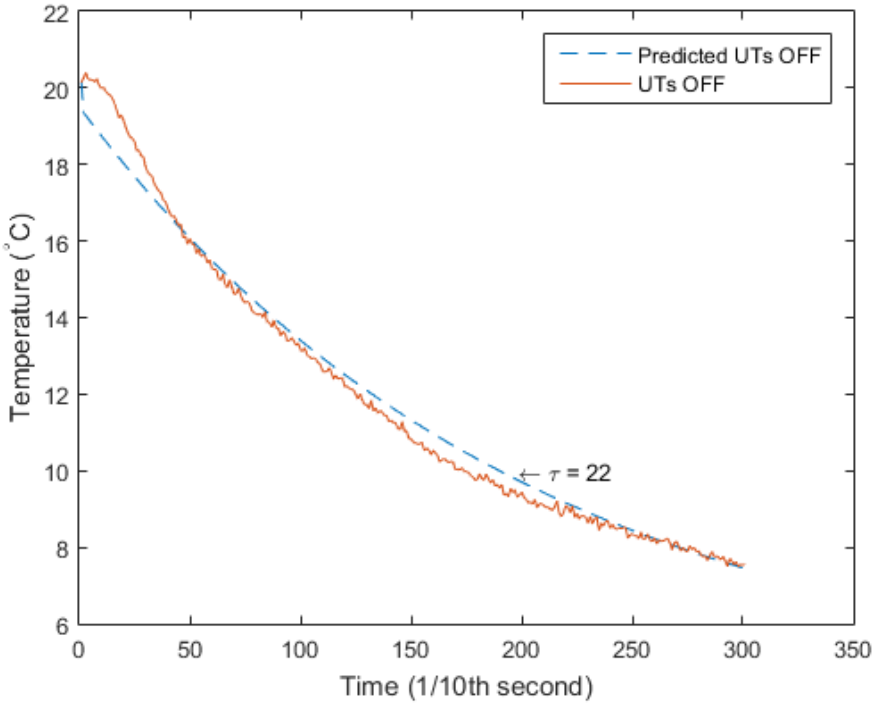


Figure 52 Temperature Time Constant Comparison: Ultrasonic Transducers Off

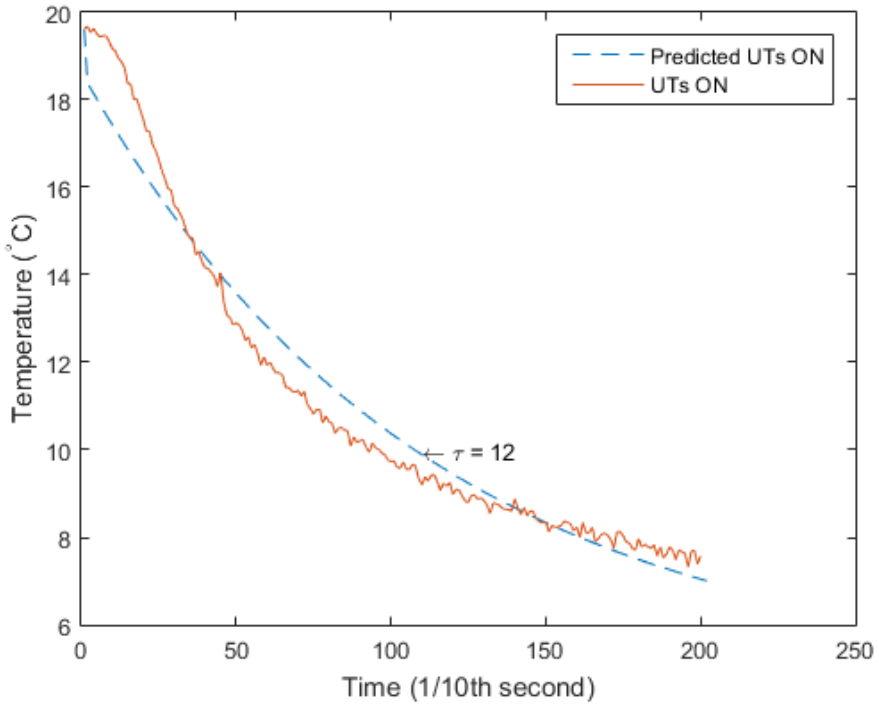


Figure 53 Temperature Time Constant Comparison: Ultrasonic Transducers ON

CONCLUSIONS

The results of this study proved ultrasonic transducers, when integrated internally to packed particle beds, improve heat transfer by up to 43%. In keeping with data in literature, the heat transfer improvements were inversely proportional to the rate of fluid flow, with the greatest improvements shown at the lower flow rates. Given that the majority of research has been focused on externally applied ultrasound as a means for heat transfer enhancements, this study indicates an opportunity for further exploration of the internal integration of ultrasonic transducers on various systems. Considering the minimal amount of power required to produce significant heat transfer improvements, the applications are wide ranging.

Future works should focus on investigating the effects of multiple ultrasonic transducers as well as the amount of power supplied to each transducer. Considering the dependence on flow rate, further research is required to determine the optimal combination of transducers, power input and flow rate. Although this study involved transient heat transfer analysis, steady-state heat transfer systems should also be investigated further. Given the ability of the ultrasonic transducers to create focused fluid streams, additional opportunities exist for research involving near-wall heat transfer analysis.

LIST OF REFERENCES

Achenbach, E. (1995). "Heat and flow characteristics of packed beds." Experimental Thermal and Fluid Science **10**(1): 17-27.

Barker, J. J. (1965). "HEAT TRANSFER IN PACKED BEDS." Industrial & Engineering Chemistry **57**(4): 43-51.

de la Fuente-Blanco, S., et al. (2006). "Food drying process by power ultrasound." Ultrasonics **44, Supplement**: e523-e527.

Gallego-Juarez, J. A., et al. (1999). "A NEW HIGH-INTENSITY ULTRASONIC TECHNOLOGY FOR FOOD DEHYDRATION." Drying Technology **17**(3): 597-608.

Gondrexon, N., et al. (2010). "Intensification of heat transfer process: Improvement of shell-and-tube heat exchanger performances by means of ultrasound." Chemical Engineering & Processing: Process Intensification **49**(9): 936-942.

Legay, M., et al. (2012). "Improvement of heat transfer by means of ultrasound: Application to a double-tube heat exchanger." Ultrasonics Sonochemistry **19**(6): 1194-1200.

Winterberg, M. and E. Tsotsas (2000). "Impact of tube-to-particle-diameter ratio on pressure drop in packed beds." AIChE Journal **46**(5): 1084-1088.

Yakhnin, V. Z. and M. Menzinger (1998). "Moving hot spots and resonance in adiabatic packed-bed reactors." AIChE Journal **44**(5): 1222-1225.

F. Baffigi and C. Bartoli, “Heat transfer enhancement from a circular cylinder to distilled water by ultrasonic waves in subcooled boiling conditions,” in Proceedings of the ITP2009 Interdisciplinary Transport Phenomena VI: Fluid, Thermal, Biological, Materials and Space Sciences, Volterra, Italy, October 2009.

J. H. Jeong and Y. C. Kwon, “Effects of ultrasonic vibration on subcooled pool boiling critical heat flux,” Heat and Mass Transfer, vol. 42, no. 12, pp. 1155–1161, 2006.

S.W.Wong andW. Y. Chon, “Effects of ultrasonic vibrations on heat transfer to liquids by natural convection and by boiling,” AIChE Journal, vol. 15, no. 2, pp. 281–288, 1969.

T. Inada, X. Zhang, A. Yabe, and Y. Kozawa, “Active control of phase change from supercooled water to ice by ultrasonic vibration 1. Control of freezing temperature,” International Journal of Heat and Mass Transfer, vol. 44, no. 23, pp. 4523–4531, 2001.

B. Li and D. W. Sun, “Effect of power ultrasound on freezing rate during immersion freezing of potatoes,” Journal of Food Engineering, vol. 55, no. 3, pp. 277–282, 2002.

Lin, Chien-Nan, “Heat transfer enhancement analysis of a cylindrical surface by a piezoelectric fan,” Applied Thermal Engineering, Vol.50(1), pp.693-703, 2013

Yao, Ye; Zhang, Xingyu; and Guo, Yiying, "Experimental Study on Heat Transfer Enhancement of Water-water Shell-and-Tube Heat Exchanger Assisted by Power Ultrasonic," International Refrigeration and Air Conditioning Conference, 2010

W.Reichelt, Chem. Ing. Tech. 44(8) (1972) 1068–1071

VITA

David Moseley was born in Knoxville, TN on October 2, 1984. Mr. Moseley earned his bachelor's degree in Business Administration from Furman University in 2007. He has owned two separate companies and has extensive experience in business development and entrepreneurship. He is a member of Tau Beta Pi engineering honor society and is passionate about technology innovation. After finishing his Master's in Mechanical Engineering and MBA in 2016, Mr. Moseley will move to Hartford, CT to work as a Component Improvement Program Manager at Pratt and Whitney.